

# We are IntechOpen, the world's leading publisher of Open Access books Built by scientists, for scientists

6,900

Open access books available

186,000

International authors and editors

200M

Downloads

Our authors are among the

154

Countries delivered to

TOP 1%

most cited scientists

12.2%

Contributors from top 500 universities



WEB OF SCIENCE™

Selection of our books indexed in the Book Citation Index  
in Web of Science™ Core Collection (BKCI)

Interested in publishing with us?  
Contact [book.department@intechopen.com](mailto:book.department@intechopen.com)

Numbers displayed above are based on latest data collected.  
For more information visit [www.intechopen.com](http://www.intechopen.com)



# Optical Fiber Sensors

Marcelo M. Werneck<sup>1</sup> and Regina Célia S. B. Allil<sup>1,2</sup>

<sup>1</sup>*Federal University of Rio de Janeiro-Instrumentation and Photonic Laboratory-Electrical Engineering Program-COPPE*

<sup>2</sup>*Brazilian Army Technology Center-Biological Defense Laboratory-Chemical, Biological and Nuclear Defence Division  
Brasil*

## 1. Introduction

Telemetry is a technology that allows remote measurement and monitoring of data. It normally refers to one-way direction of information, that is, from the sensor to the interrogation system or data logger system. Telemetry could be defined as a sub-class of telecom, a more complex way of exchanging information such as Internet, telephone calls or video transmission.

Telecommand, the counterpart of telemetry, occurs when the remote systems require remote instructions and data to operate, which means that the information goes on the other direction.

Telemetry finds applications in aerospace, automotive, consumer, engineering, industrial manufacturing, medical, military, electric power industry etc.

Although the term telemetry commonly refers to wireless data transfer mechanisms (e.g. using radio or infrared systems), it also encompasses data transferred over other media, such as a telephone or computer network, optical link or other wired communications.

In the applications mentioned above and particularly in the electric power industry, we find normally protocols that can be either bidirectional or mono directional, such as Fieldbus, RS-485, Ethernet, 4-20 mA, 0-10 V, all working in a twisted-pair basis. These protocols, although being among us for many decades, have disadvantages, particularly when applied to the electric power industry. One of these disadvantages is that data transmitted through electric wires normally need electric energy at the sensor end, or in other words, the transducer needs to be powered in order to measure and transmit data. However, it occurs that sometimes providing electric energy at the sensor location is difficult for it could be far away from any appropriated power supply. This happens in long high voltage transmission lines or along pipe-lines or in deep ocean, for instance. The other problem with these protocols is that they electrically connect the sensor location with the interrogation location. The main consequence of this is that short circuits due to malfunctioning or atmospheric discharges can easily be transferred to the operation room and furthermore putting the substation personnel and equipment at risk.

With the invention of the practical optical fiber in the 70's the world watched a boom in the telecommunication technology. In the 80's, with the popularity of optical fiber technology, scientists started to develop a new class of sensors and transducers: the optical fiber sensors. They came offering many advantages over the other technologies and soon started to be applied in telemetry with very good return in costs, maintenance and efficiency.

In conclusion, when it comes to telemetry, optical fibers perform telemetric measurements at distances much longer than conventional telemetry protocols and media. Additionally, due to its virtually infinite capacity to multiplex, one can mix different kinds of signals in one single fiber therefore saving many kilometers of copper wires, which is also welcome by the maintenance personnel.

In this article we will concentrate on applications of telemetry over optical fiber and on optical fiber sensors which encompass telemetry and sensor in one single media.

## 2. Optical fiber sensors

Optical fiber sensors (OFS) came just after the invention of the optical fiber in the 70's. At the beginning of this era, optical devices such as laser, photodetectors and the optical fibers were very expensive, adequate only to the already saturated telephone network in which companies would pay any price to transmit more information and more telephone calls. With the great diffusion of the optical fiber technology in the 80's and on, optoelectronic devices became less expensive, what favored their use in OFS.

OFS can be applied in many branches of the industry but we will concentrate here their applications through our experience in the electric power industry.

In this area, the operators need to measure and monitor some important physical parameters that include:

- Strain ( $\mu\epsilon$ )
- Vibration of structures and machines
- Electric current (from A to kA)
- Voltage (from mV to MV)
- Impedancy ( $\mu\Omega$ )
- Leakage current of insulators ( $\mu\text{A}$  to mA)
- Temperature
- Pressure
- Gas concentration
- Distance between stationary and rotating or moving parts

Some of these parameters, depending on where they are located, are very difficult or even impossible to be conventionally monitored because of a well-known paradigm of the electrical power industry: An electric sensor cannot be close enough to a high potential in order to break the electric rigidity of the air, which is about 1 kV/cm. This would cause a short circuit when the current would flow from high voltage to ground potential by the sensor's connecting wires. The best option to avoid this catastrophic effect is the OFS, because the fiber is made of dielectric materials and therefore it is possible to be placed very close or even touch a high potential conductor and they do not necessary need electrical power at the sensor location.

OFS can be built using several physical principles and materials. They have specific characteristics that are well exploited when applied to the electric power industry and in this case OFS offer a large number of advantages over conventional sensors. The most important are:

- High immunity to EMI
- Electrical insulation
- Absence of metallic parts
- Local electrical power not required
- Lightweight and compactness

- Easy maintenance
- Chemically inert even against corrosion
- Work over long distances
- Several sensors can be multiplexed on the same fiber

The high immunity to electromagnetic interference (EMI) is a strong requirement for sensing in electromagnetic contaminated environments, e.g. RF-field and high electric and magnetic fields present in power lines.

The insulation is another special requirement, because as these sensors are inherently electrically insulated (dielectric) and do not require external power, this means that there is no electric path from the power line to ground, which means high personnel security. Therefore the optical fiber sensors can work at high electrical potentials and in potentially explosive environments.

Optical fibers can be used as sensors by modifying a fiber so that the measurand interferes on the guided light and modulate light parameters such as intensity, phase, polarization, wavelength, or transit time of light over the fiber. Sensors that vary the intensity of light are the simplest, since only a simple source and detector are required.

We can divide OFS in three basic categories: intrinsic, extrinsic and evanescent field based.

Extrinsic fiber optic sensors use an optical fiber, normally multi-mode, to transmit modulated light from either a non-fiber optical sensor or an electronic sensor connected to an optical transmitter. In this case the optical fiber is used only to transmit light to and from the sensor. This kind of sensor sometimes is called hybrid sensor for it encloses different technologies such as optics and electronics.

In intrinsic sensors the light does not leave the fiber and the light modulation takes place inside the fiber. This kind of sensor presents the major benefit to have the ability to reach otherwise inaccessible places and without the need of electrical energy at the sensing location.

The third category is the evanescent field based sensor. Due to the total internal reflection phenomenon that occurs in the core-cladding interface of the fiber, the light propagating in the fiber has two components - an oscillatory field in the core and an exponentially decaying field in the cladding. The latter field, referred to as the evanescent field, is the key to sensing and is based on the modulation of the light amplitude in the core of the fiber by the optical properties of the surrounding medium.

When developing an OFS we can use the fiber for: a) conducting light; b) to be the sensor itself; and c) for both applications, that is, sensing and conducting light to and from the sensing area.

An optical fiber is a thin, flexible, transparent glassy filament that acts as a waveguide, or "light pipe", to transmit light from the light source to the photodetector located at the two ends of the fiber. They are mainly used for telecom and sensing but find many uses in the industry, research sciences, medicine, entertainment etc.

By the 70's all telephone cables and microwave links in the planet were already saturated. The solution came when Charles Kao and George Hockham of the British company Standard Telephones and Cables (STC) promoted the idea that the attenuation in the existing optical fibers could be reduced below 20 decibels per kilometer (dB/km), making fibers a practical communication medium. They proposed that the attenuation in fibers available at the time was caused by impurities that could be removed by chemical processes. They correctly and systematically theorized the light-loss properties for optical fiber, and pointed out the right material to use for such fibers — silica glass with high purity. This discovery earned Kao the Nobel Prize in Physics in 2009.

The crucial attenuation limit of 20 dB/km was first achieved in 1970 by researchers at the American glass maker Corning Glass Works, now Corning Incorporated. They demonstrated a fiber with 17 dB/km attenuation by doping silica glass with titanium. A few years later they produced a fiber with only 4 dB/km attenuation using germanium dioxide as the core dopant. Such low attenuation allowed optical fiber to be used in telecom from the 80's until today when the telecom fiber presents an attenuation of only 0.25 dB/km. Although polymeric optical fibers (POF) are around us much longer than silica fibers, only in the last decade they start to attract attention for LANs and small industrial networks and their use for sensors has just emerged few years ago. Figure 2.1 shows the different diameters as comparing POFs with silica fibers.



Fig. 2.1. Relative comparison of diameters in different kinds of fibers. SI-POF=step-index polymeric optical fiber; PCS=plastic cladding silica fiber; MM Silica=multimode silica fiber; SM silica=single mode silica fiber; PF-GI-POF=perfluorinated graded-index POF. The light color represents the cladding and dark color the core.

The first report of poly-metil-meta-acrylate (PMMA) POF dates from 1968 when Du Pont presented a POF with an attenuation of 500 dB/km. From then on several laboratories are keeping trying to decrease the attenuation in order to apply POF in telecom. Figure 2.2 shows the results of those efforts.

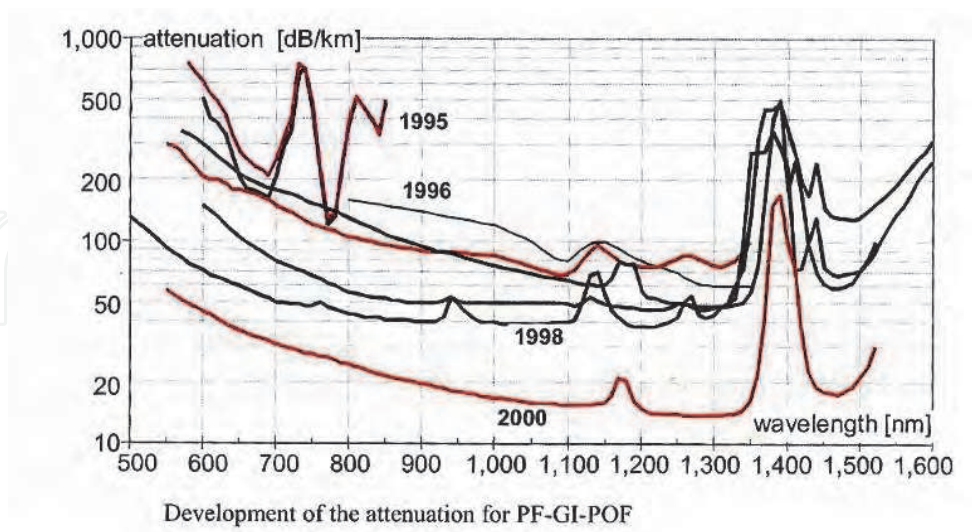


Fig. 2.2. History of the attenuation improvement of PF-GI-POF.

Comparing POF and silica fibers by the attenuation, silica fibers are much better. However, when constructing a fiber sensor using POF instead of silica, we have some additional advantages:



- Maintenance costs
- More resistance to strain
- Cheaper peripheral components
- Easy handling
- No need of special skill for splicing and connectorization

Due to their larger diameter, it is simpler to work with open optics and easy handling. POFs are cheaper than their counterpart as well as the peripheral components and devices, such as connectors, LEDs and photodetectors. They also present more resistance to strain (larger modulus of elasticity) which means more reliable networks. Finally, many interfaces can be built in laboratory what makes the maintenance cost much lower than when dealing with silica fibers.

Of course POFs have disadvantages too. POF only transmits visible and near infrared light, so we cannot use the available technology of telecommunications such as 1300 nm and 1500 nm telecom windows. Additionally, POF has a very high attenuation in the visible spectrum (see Fig. 2.3).

The other issue is the temperature because plastic materials cannot withstand high temperatures as much as glasses. POFs can operate only up to 70 to 85°C. However, some specials POFs have been developed mainly for harsh environment such as in car networks. In these applications POFs have to withstand temperatures as much as 150°C. Table 1 shows some examples.

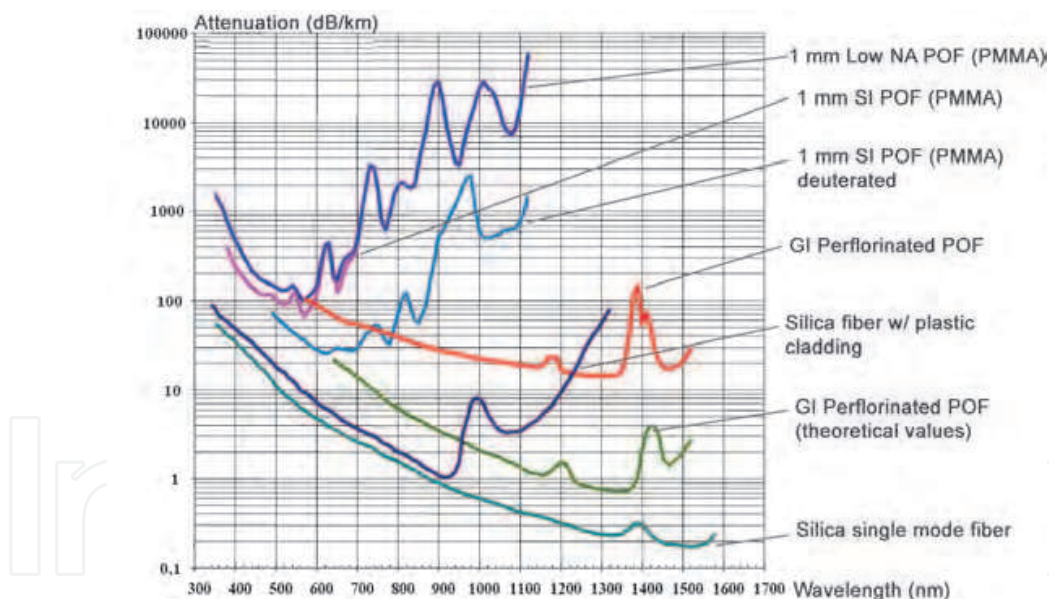


Fig. 2.3. Optical attenuation of silica fibers and POFs.

The attenuation of silica fibers is negligible for sensing distances (around 1 km), but when using a POF for transmitting light, the first thing to have in mind is the high attenuation the POF impinges to the light.

### 3. Case studies

This section will present real applications of OFS and telemetry in the electrical power industry. The techniques presented here have been tested in the field mainly in high voltage

transmission lines, in substation equipments and in hydroelectric generators, all in a connected-to-the-grid basis.

### **3.1 Application of POF and ruby for temperature measurement in an electric power substation**

#### **3.1.1 Introduction**

Temperature is a very important parameter for the electric power industry because insulators, copper conductors, iron core of transformers, insulating oil and every equipment are very sensitive to the temperature which has to be kept under strict control during all times. Nevertheless, when dealing with high voltage, sometimes one cannot use conventional electric sensors particularly when working near high voltage areas. This case reports the development of a temperature sensor system using the fluorescence technique.

The fluorescence effect can be used as an indicator and generate a signal proportional to a specific parameter need to be monitored. In the same way, fluorescent materials can be used as sensors. It is well known that the fluorescence decay time of some crystals is proportional to the temperature. Therefore, one way to build a temperature sensor is by the measurement of the time constant of the exponential decay that produces a linear relationship with the temperature.

Optical fibre sensors offer a large number of advantages over conventional sensors such as high immunity to electromagnetic interference, electrical isolation and the absence of metallic parts, a strong requirement for sensing in electromagnetic contaminated environments, e.g. RF/microwave. The sensor probes are inherently electrically insulated system and external power is not required for their operation, they can work at high electrical potentials and in potentially explosive environments. It can be made as lightweight, compact, disposable of low cost and is highly chemically inert even against corrosion.

The fluorescence based sensors offer the advantage of a near-zero background, because the wavelength of the emitted light is always larger than that of the excitation light, which makes then in principle much more sensitive and error immune than those that change only the absorption when the temperature varies [Asada and Yuki, 1994, Grattan and Zhang, 1995]. Previously, experiments with commercial polystyrene fluorescent fibres as temperature sensor were done [Ribeiro et al., 2003]. Although it features some advantages as compatibility with standards POFs, a weak fluorescence signal with time-decay  $< 100$  ns was measured, thus requiring a much complex electronics. Furthermore, the polystyrene can withstand only up to  $\sim 70^\circ\text{C}$  thus limiting its usefulness for the electrical energy industry. Ruby has been used for fluorescence thermometry because it is of low cost, easily available, POF compatible, requires low cost source (blue or green ultra-bright LEDs), Si-based photodetection and simple electronics. Additionally it presents strong intensity and long lifetime of fluorescence signal. The fluorescence peaking at 694 nm wavelength features a long-decay time of 2-4 ms. Persegol and co-workers [Persegol et al., 1999] described a POF-based temperature sensor in the range  $-20^\circ\text{C}$  to  $+120^\circ\text{C}$  with an accuracy of  $\pm 2^\circ\text{C}$  for early detection of faults in medium-voltage (36 kV) substations. They used heavily-doped ruby powder packaged at the POF end as fluorescent material pumped with a green LED. Two POF-probe were used, one for pumping the ruby and the other for bringing the fluorescence back to the photodetector.

In this case study we describe the temperature sensor prototype development based on the ruby crystal and a one-probe-POF for “low” and “high” temperatures. Low cost passive and active components as couplers, connectors, adapters, LEDs etc were used. Ruby crystals are

geometrically compatible with standard POFs and even after cutting and polishing it remains at low cost.

### 3.1.2 The prototype

Fig. 3.1.1 shows a top view picture of the temperature sensor prototype (conditioning equipment) where the key components are assigned. The LED package was polished almost reaching the semiconductor chip thus maximizing the light caption. Light launching was made through butt-coupling the polished LED and a carefully terminated POF. Optical pulses of 32 ms time-width from the LED were generated to pump the ruby crystal at 15.6 Hz. A miniature 1x2 POF-coupler is used to send pump pulses toward the ruby crystal glued at the end of the POF-probe and to collect the fluorescence toward the Si-photodetector.

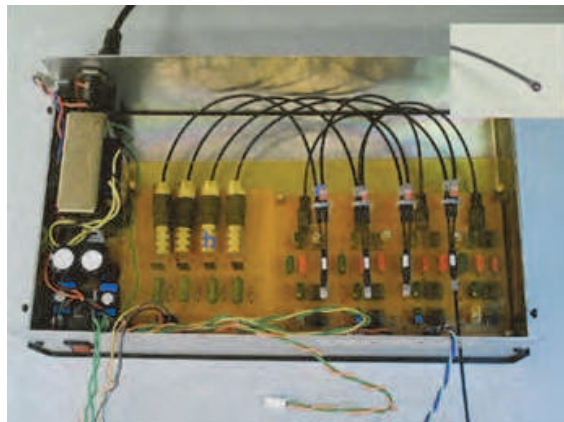


Fig. 3.1.1. Top view picture of the temperature sensor prototype (conditioning equipment).

Fig. 3.1.2 shows the picture of the one-POF-probe with 4 mm in diameter. The POF was terminated at the other end with a standard HP plastic connector. With this configuration, it can be detached from the conditioning equipment box. The fluorescence response from the crystal, passing through the same POF, was conveyed into the other port of the coupler. Due to the back reflections at the many optical interfaces, the fluorescent signal could have been buried under the intense excitation signal. Thus, in order to avoid a saturation of the detection stage and to enable the fluorescence response to be detected exclusively, a red long-pass filter was placed before the Si photodiode. The electrical signal generated from the photodiode is amplified and processed.

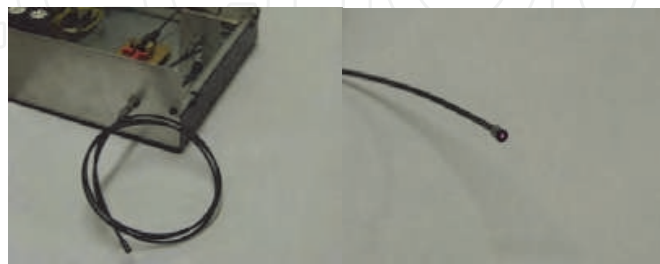


Fig. 3.1.2. Picture of the miniaturised POF-probe with hemispherical ruby crystal.

The field prototype probe (Fig. 3.1.3) was designed to work in the field under 25 kV. The POF with the ruby crystal is inserted inside the probe up to its tip where it touches the copper conductor of the coil.





Fig. 3.1.3. High voltage probe.

3.1.3 Prototype tests

Fig. 3.1.4 shows in the top the oscilloscope trace of the square shape pump pulses. Bottom trace shows the fluorescence signal at room temperature exhibiting a clear exponential time-decay.

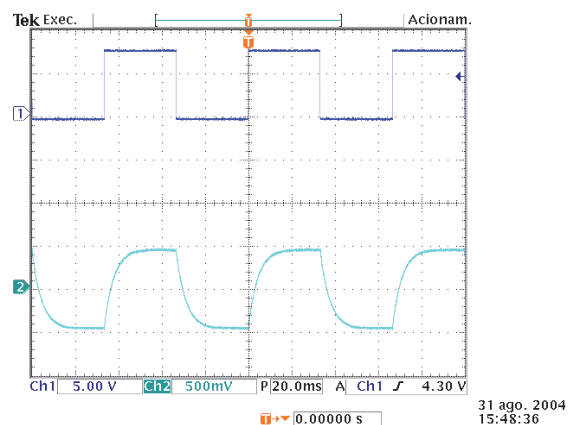


Fig. 3.1.4. Oscilloscope traces of pump (top) and fluorescent (bottom) light signals at room temperature (23°C).

The exponential decay shown in Fig. 3.1.4 can be expressed as:

$$P(t) = P_0 \exp[-t/\tau(T)]$$

where  $P(t)$  is the output light power at a time  $t$ ,  $P_0$  is the light power at  $t=0$  and  $\tau(T)$  it the time-decay constant at temperature  $T$ . Fig 3.1.5 shows the measurements of fluorescence time-decay  $\tau$  against the temperature  $T$  with a typical relaxation time of about 5.0 ms.

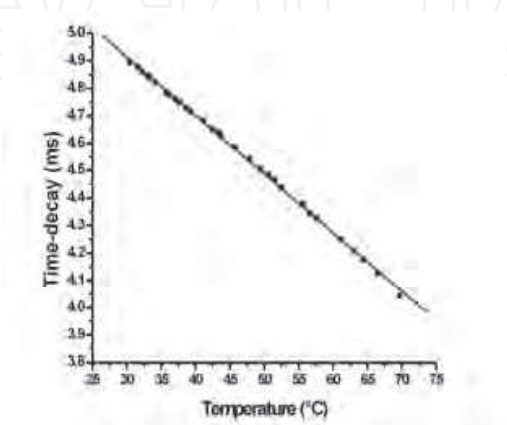


Fig. 3.1.5. Fluorescence time-decay against the temperature.

From the straight line slope shown in Figure 3.1.5 the sensitivity is calculated to be 22.5  $\mu\text{s}/^\circ\text{C}$  corresponding to an estimated temperature resolution of  $\sim 1^\circ\text{C}$ . A sensitivity of 9  $\mu\text{s}/^\circ\text{C}$  has been reported in the literature. However, our sample presented a larger sensitivity probably due to the re-absorption phenomena [Persegol et al., 1999].

Plastic materials cannot withstand high temperatures as much as glasses. Standard POFs usually can operate up to 70 to 85 $^\circ\text{C}$ . However, some special POFs have been developed mainly for harsh environment as in car networks applications. Some of those “high-temperature” POFs had been disclosed in the literature but still impose severe limitations for temperature sensing [Ribeiro et al., 2003].

Table 1 shows the attenuation given by the manufacturer for three POFs (Mitsubishi Rayon Company) corresponding to centre wavelengths of blue/green LEDs and ruby R-line (694 nm).

Fiber Type	470 nm	525 nm	694 nm
EH4001 (datacom-grade)	$\sim 0.10\text{ dB/m}$	$\sim 0.10\text{ dB/m}$	$> 0.40\text{ dB/m}$
DH4001 (heat-resistant, 115 $^\circ\text{C}$ )	$0.95\text{ dB/m}$	$0.48\text{ dB/m}$	$0.40\text{ dB/m}$
FH4001 (heat-resistant, PC core, 125 $^\circ\text{C}$ )	$4.00\text{ dB/m}$	$2.70\text{ dB/m}$	$1.30\text{ dB/m}$

Table 1. Attenuation of three POFs at some key wavelengths. PC = polycarbonate.

From Table 1 one can see that the EH4001 POF-probe attenuation is the same despite the use of blue or green LED regarding a maximum temperature of 85 $^\circ\text{C}$  for which this POF can withstand.

Table 2 shows comparatively the attenuations for 10m of POF-probe length when a maximum temperature of 110 $^\circ\text{C}$  is allowed to be reached.

	470 nm (pump) + 694nm (fluorescence)	525 nm (pump) + 694nm (fluorescence)
EH 4001	$1.0 + 4.0 = 5.0\text{ dB}$	$1.0 + 4.0 = 5.0\text{ dB}$
DH4001	$9.5 + 4.0 = 13.5\text{ dB}$	$4.8 + 4.0 = 8.8\text{ dB}$
FH4001	$40.0 + 13.0 = 53.0\text{ dB}$	$27.0 + 13.0 = 40.0\text{ dB}$

Table 2. Attenuation for 10 m of POF-probe for different pump wavelengths.

Fibers type DH4001 and FH4001 can withstand up to 115 $^\circ\text{C}$  and 125 $^\circ\text{C}$ , respectively. However, our choice as “high temperature” POF-probe was the heat resistant-grade DH4001 (1 mm core with black XPE jacket) because it features total attenuation of 8.8 dB that is much smaller than 40.0 dB presented by FH4001 regarding the green LED as the excitation light source.

3.1.4 Field installation

The system has been installed at the harmonic filter of Furnas Substation in the city of Ibiúna, State of São Paulo, Brasil to allow the technicians to monitor the temperature in four points of the coil of this reactor in real time. If the temperature reaches 80 $^\circ\text{C}$  an alarm is issued in order to shut down the transmission line. Fig 3.1.6 shows one of the four installed sensors, Fig. 3.1.7 shows the coil with two of the sensors and Fig. 3.1.8 shows the control software which screen shows the graph of the four temperatures as well as the ambient temperature.



Fig. 3.1.6. One of the four sensors installed on the top of the coil.



Fig. 3.1.7. The reactor coil and the sensors installed.

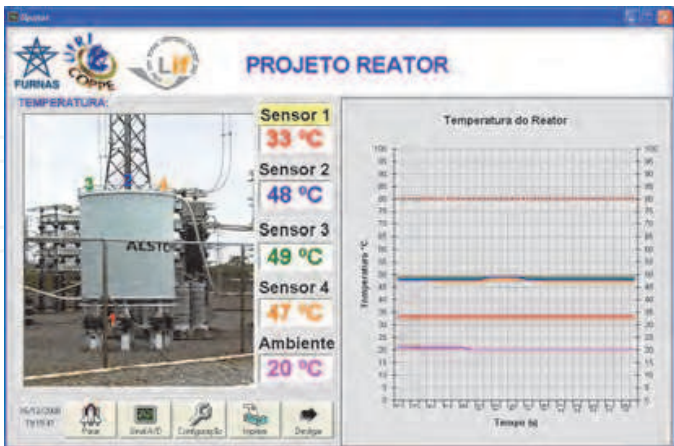


Fig. 3.1.8. Control software screen showing the graph of the four temperatures as well as the ambient temperature.

**3.1.5 Results**

Figures 3.1.9 and 3.1.10 show the graphs of the measurements taken at two different dates.

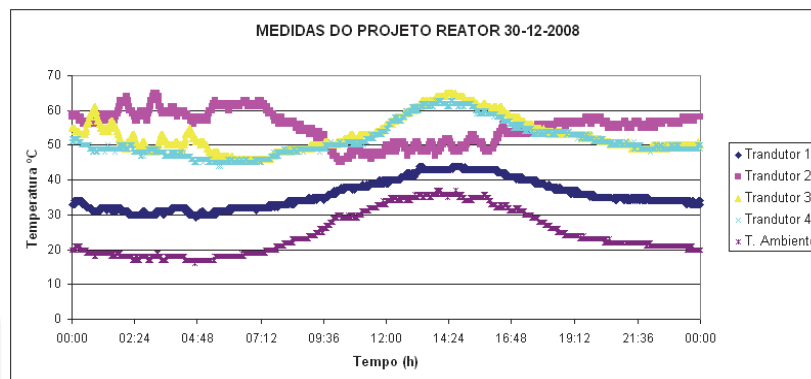


Fig. 3.1.9. Temperature monitored by the four transducers.

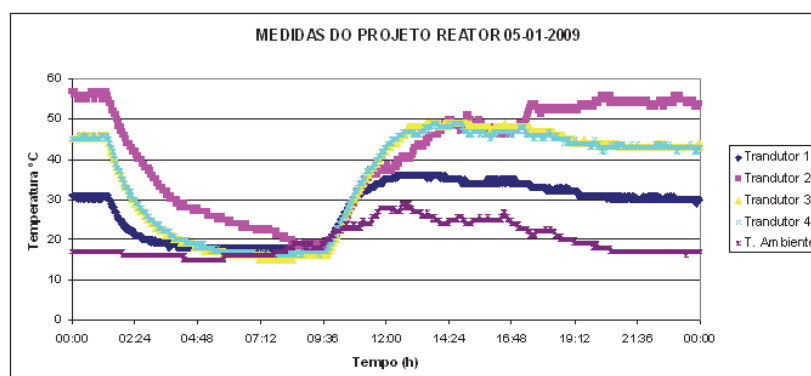


Fig. 3.1.10. Temperature monitored during an electric power shortage.

### 3.1.6 Concluding remarks

Experimental results of a simple and low cost four-point temperature POF sensor prototype based on time-decay of the ruby fluorescence pumped with blue (or green) ultra-bright LED are presented. The major drawbacks of polymer optical fibres are their restricted temperature range and relatively high losses. However many applications do not exceed a temperature of more than 100°C and requires a sensing distance smaller than 10 m. The best choice for temperatures up to 115°C was the DH4001 as the POF-probe pumped with green LED. The developed prototype is quite compatible with a 1-mm-core silica fibre or a hybrid POF + silica fibre-probe where the later may be put in contact with the hot surface to be sensed.

## 3.2 Application of a POF-based current sensor for measuring leakage current in 500 kV transmission line

### 3.2.1 Introduction

The leakage current of insulators in a high voltage transmission line is due to the increasing conductive deposited yielded by environment pollution. The more common pollution is the salt-spray produced by winds in areas close to sea shore. The salt deposit on the insulator surface offers to the electrical current alternative paths to the ground, thus connecting the high voltage to ground potential. Although this current is only a few tens of milliamperes, when multiplied by the total number of insulators located in that particular transmission line, the total leakage current can reach so high values that can trigger over current protection devices leading to electrical power line interruption. When an electric arc occurs,



it is called “flashover”, leading occasionally to the destruction of the whole insulator [Kanashiro and Burani, 1996].

An optoelectronic sensor for real time leakage current monitoring of high-voltage (500kV) power lines insulators was developed as a continuation of a study presented on the 2003 POF Conference (Werneck et al, 2003). The leakage current drives an ultra-bright green LED. The optically intensity-encoded data measurement is coupled to a POF and transmitted from the high potential to ground potential. After demodulation, the RMS value of the leakage current and waveforms are sent to a remote station using a GPRS code in a cell-phone platform. This case study shows the sensing system, the telemetry technology and the results obtained.

The continuous monitoring of leakage current levels yields parameters to establish an operational preventive strategy of cleaning or substitution of insulators placed inside the area with favorable conditions to flashover occurrence.

Usually, in order to monitor leakage current, it is applied a resistor (Briggs, 1976; Amarh, 2001) or an induction coil (Maraio, 1992). However, these methods need the connection to potential, allowing electromagnetic interference and risks to personnel. In order to circumvent this problem it has been proposed the development of an optoelectronic system using plastic optical fiber (POF) technology. This method has some advantages, such as it does not suffer electromagnetic interference effect; it is of low cost, light weight and does not need power supply to work.

With this system in operational status it will bring benefits such as energy losses monitoring and increasing the grid reliability. It also promotes optimization of insulators washing causing therefore a reduction of maintenance cost.

### 3.2.2 System description and methods

The sensor previously developed and presented in the 2003 POF Conference was used for 13.8 kV whereas this same technology is now used for a 500 kV transmission line in the city of São Luis, State of Maranhão, Brazil. Fig. 3.2.1 shows the schematic diagram of the system.

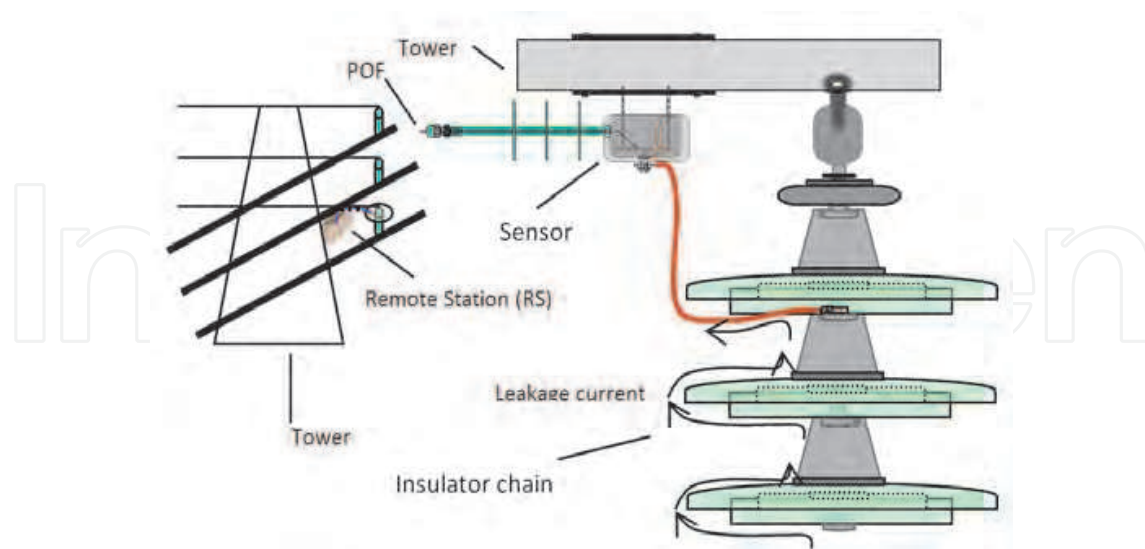


Fig. 3.2.1. Schematic diagram of the system

The main problem is the insulation of the whole system, since at this so high voltage, nearly everything conducts, including POFs. Therefore, we should place the sensor at or near ground potential.



The method proposed to monitor the leakage current of high-voltage circuits is based on the fact that all leakage current flows through all insulator sectors (see Fig. 3.2.1). Therefore if we measure the current from the last section of the insulator to ground, we are actually measuring the leakage current and with the sensor connected at a low voltage level. Fig. 3.2.2 shows the location where the control and transmission box is installed and the location where the sensor is installed at the insulator chain of a 500 kV transmission line tower.

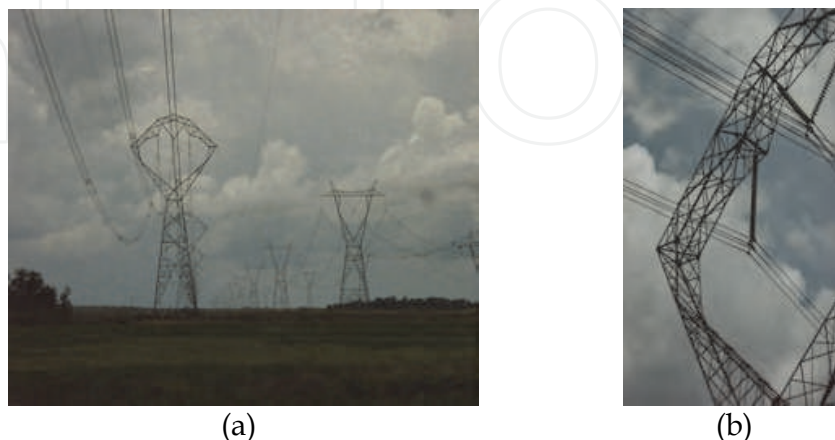


Fig. 3.2.2. The arrows show the location where the control and transmission box is installed and the location where the sensor is installed.

### 3.2.3 The transducer

The leakage current supplies energy enough to optically power a high efficient blue-green-LED (Marcou, 1997). The leakage current modulates the LED output power that is transmitted to the receptor by means of a specially protected POF. The emitted light from the LED is amplitude and wavelength modulated. In this work it was applied only amplitude modulation/demodulation technique.

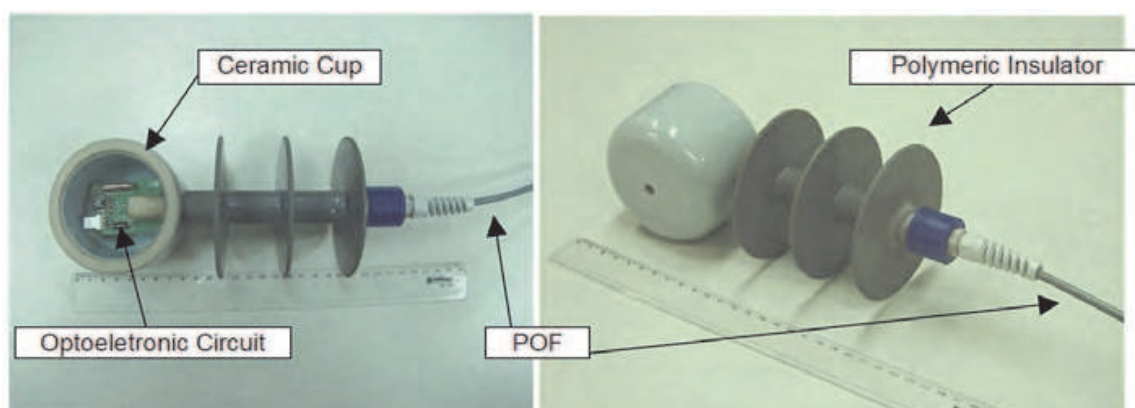


Fig. 3.2.3. Picture of the POF-based leakage current sensor

The optical signal is detected by the receptor circuit, inside the Remote Station that performs the half cycle demodulation. Fig. 3.2.3 shows pictures of the transducer which was designed to be connect to the test-insulator. Calibration and measurement procedures of leakage waveforms were made under controlled laboratory conditions by a salt-spray chamber aiming to simulate the real conditions of the field.

### 3.2.4 Remote station

The Remote Station contains the sensor interrogation system the CPU and the cell-phone transmitter. The electronic hardware is composed by the followings modules: CPU board associated to the datalogger system; power supply; battery and cell phone (see Fig. 3.2.4).

The RS, designed to work under field conditions, is attached at the metallic structure located at medium height of the tower (see Fig. 3.2.2a).

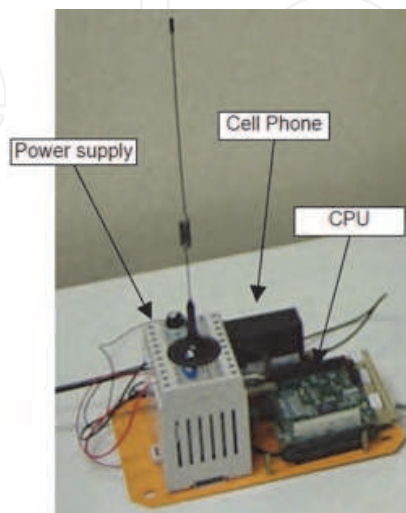


Fig. 3.2.4. Electronic hardware inside of Remote Station: power supply, battery, datalogger, CPU and cell phone.

### 3.2.5 The software

The software is responsible for establishing the communication between RS (installed in field) and any authenticated computer connected to the Internet. The signals are acquired, processed and stored in memory. In another cycle, the data is sent to the remote computer via modem. Another program is responsible for remote updates of the local software. This feature is particularly important because the monitoring place is about 2000 km away from the Laboratory and very often a new update of the local program has to be installed in the system and this is done remotely. Fig. 3.2.5 shows the remote screen as seen in our laboratory.



Fig. 3.2.5. Main screen to be monitored by the Internet.

### 3.2.6 Results

The monitoring process is based on block dataset transference, which is related with values sampled from specific time interval. Figure 3.2.6 shows a set of data downloaded from the system's website.

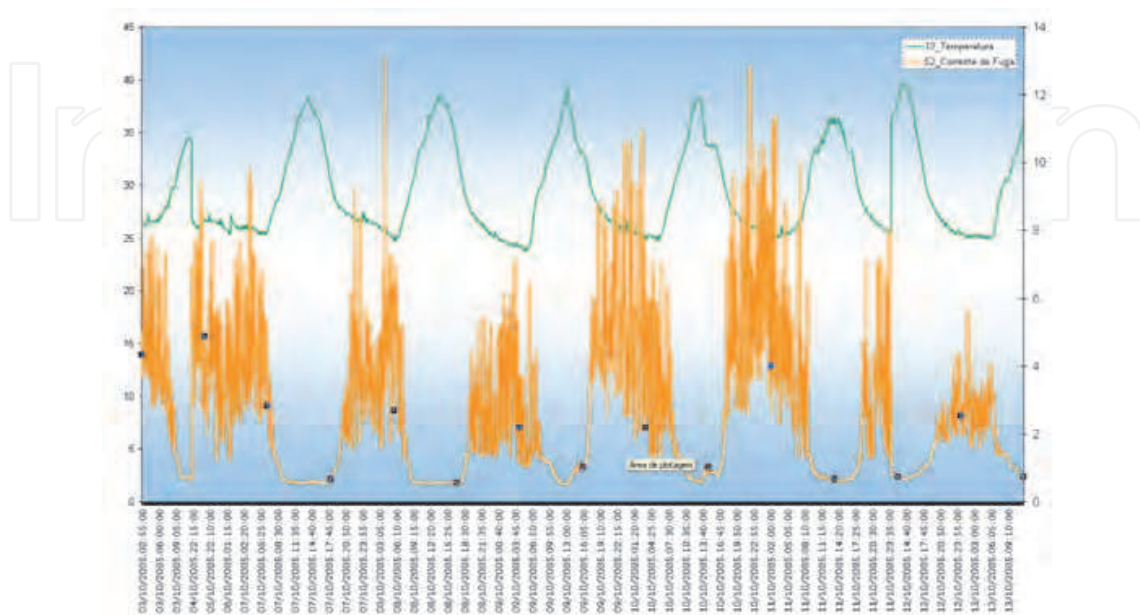


Fig. 3.2.6. Results downloaded from the system's website. The upper trace is the ambient temperature and the lower trace is the leakage current.

### 3.2.7 Discussion and conclusions

The LED/POF technology applied in the leakage current sensor presents some advantages over other techniques adopted in last years, i.e.: efficient, easy to handle, robust and reliable. Despite problems described on the literature, optical amplitude modulation technique applied to fiber optic sensing proved to be efficient enough to obtain the leakage current so that the use of frequency modulation technique proposed as alternative technique was not necessary (Culshaw & Dakin, 1989 and 1997).

The objectives of this project were reached, however, in order to this technique be of any usefulness to the company, it is necessary to transform the data into information. This means to establish parameters which can determinate the real status of the insulator regarding the leakage current allowed to flow to the ground. After such parameter has been established, it will be possible to issue the "washing procedures" alarm, meaning that if the set of insulators were not washed immediately, a flashover may occur. The establishment of these parameters would produce the logistic insertion of this activity in company, reducing the risk probability of an insulator failing. To create these parameters it would be necessary to analyze a great diversified amount of data from different critical points of maritime pollution inside the company operation area. Thus, it would be possible to determinate the optimum point to intervention (washing of insulators). On the other hand, it could be possible to establish an analytical relationship between different kinds of insulators under same pollution conditions, aiming at the creation of a "performance indicator" to each insulator under the same conditions. This analytic methodology could supply most adequate insulator to specific geo-meteorological region.

### **3.3 Hybrid optoelectronic sensor for current and temperature monitoring in overhead transmission lines**

#### **3.3.1 Introduction**

Transmission line (TL) capacity is determined by the maximum power transmitted from the source to the load. Since the line voltage is always fixed, this capacity is in fact the maximum current capable to flow in the TL. Normally, during the project, this maximum power is established and the whole project is built around this parameter. When the energy demands grow, technicians are worried to infringe standards of security and performance, such as wire temperature and sag (conductor-to-ground distance).

The sag is a very important parameter since it is directly related to the current: the higher the current, the higher the conductor temperature, and so thermal expansion, consequently decreasing the conductor-to-ground distance. Nevertheless, the conductor temperature does not depend only on the electrical current. It is strongly dependent on environmental features such as wind velocity and direction, ambient air temperature, pollution, cable construction, rain and snow conditions [Douglas and Thrash, 2007]. So, TL maximum sag characteristic is determined always considering the worst case aiming the best safety conditions.

With the increasing demand for electrical energy, especially in developing countries, the idea to utilize the full transmission capacity of already existing TL, instead of built new ones, is quite attractive. The idea behind this project, which will be confirmed by data collected from the system in the field, is that the temperature of the conductor depends on current and weather conditions, but the sag only depends on the conductor temperature, regardless the weather conditions.

The system operates in two stages. The first stage will provide the measurement of three parameters: line current, conductor temperature and sag. This system will be installed in one or two TL towers for sufficient period of time to acquire data at all possible situations. This information will make it feasible to establish a set of calibration curves which will relate sag distance with conductor temperature, and sag distance with line current. The sag will be measured by taken photographs of a target hung on the middle of the catenary. A neural network recognizes the target on the picture and calculates its distance from a background reference.

Since the sag is dependent on line current and conductor temperature, on the second stage of the project only current and temperature sensors will remain installed on the TL tower. Thus, technicians will be able to infer the sag value exclusively from the latter parameters. The conductor-sag distance, acquired using the digital processing of digital camera images, plus the data regarding conductor current and temperature, will enable the development of a catenary behavior estimation algorithm, for each monitored and calibrated TL conductor cable, hence eliminating the necessity of constant monitoring.

#### **3.3.2 System description**

The system is comprised of three monitoring sub-systems: a temperature sensor, a current sensor and a conductor-sag monitoring sub-system. These three sub-systems will be installed on a 138 kV transmission line tower, in order to monitor the sag between this tower and the next one, being this conductor sag a strategic and representative one. Once the effectiveness of this method is confirmed, the system will be reproduced and taken to monitor problematic sags in the company's transmission lines.

The current transformer and the temperature system are composed by two subsystems: the one in ground potential and the one in high voltage (138 kV); the latter is optically powered



by the former in the following manner: in ground potential a laser injects 830 nm light in a multimode ordinary telecommunications optical fiber. This fiber is directed to the high potential subsystem through a specially designed 138 kV polymeric insulator. At the high potential level, the laser light is converted into electric energy through a conventional silicon photodetector. This energy powers all electronic circuits embarked on the high voltage level: current and temperature sensors, microcontroller and fiber optic serial transmitter. The transmitter relays the data collected to the ground potential through another multi-mode optical fiber that is also insulated by the previously mentioned 138 kV insulator.

A Rogowski coil, a helical coil sensor uniformly wound on a relatively long non-magnetic strip [Tumanski, 2007], is used as a current sensor, which offers advantages compared to conventional current transformers, such as linearity and easy handling [Ward and Exon, 1993]. The cable temperature measurement is implemented through a conventional LM35 integrated circuit, which is very simple and inexpensive. The sensors' electrical output signals are digitalized and processed by means of a low-power microcontroller and sent to a receiving system located at the low-voltage region using a LED operating at 850 nm wavelength, connected to a multimode 62.5/125- $\mu\text{m}$  optical fiber.

### 3.3.3 Power over fiber link

All the circuits located in the high voltage area are optically powered; a laser module at the low-voltage area launches up to 1W optical power at 830 nm in another multimode 62.5/125- $\mu\text{m}$  fiber, conducting the energy to the photovoltaic power converter remotely situated. Power and data channels can be combined into a single optical fiber linking both high and low voltage areas [Böttger et al, 2008]; however, in this monitoring system for TL an option for dedicated fiber cables was made [Tardy et al, 1995 and Pember et al, 1995]. A general view of the system is presented in Fig. 3.3.1.

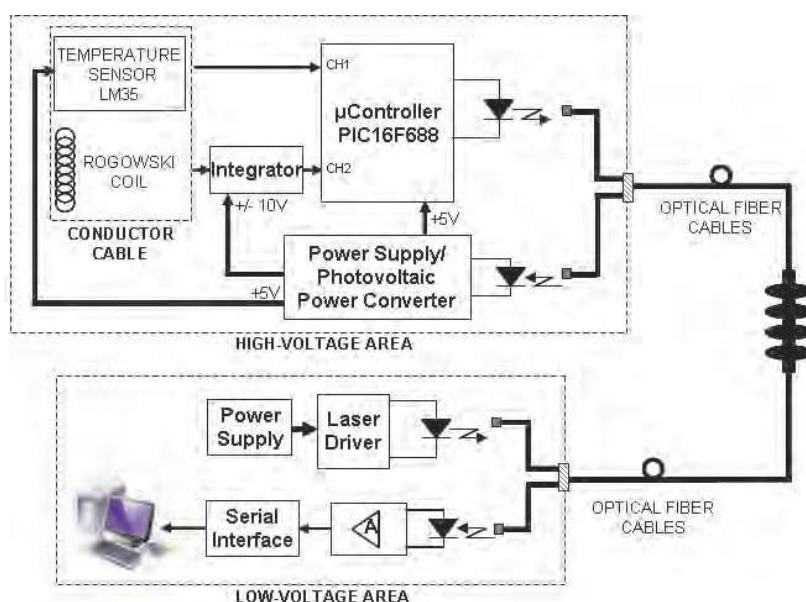


Fig. 3.3.1. General view of the system, showing the circuits situated in high and low voltage regions.

The system is comprised of the following sub-modulus: the laser module located at the low voltage region, 830 nm operating wavelength, and controlled by a driver which can manage



the launch of up to 1 W optical power; a 40m-long-62.5- $\mu\text{m}$  multimode optical fiber to guide the optical power; and a photovoltaic power converter (PPC), which is an array of semiconducting diodes.

Optical attenuation is a key issue when photonic power is used. Fiber splices and connectors were implemented to incorporate the 40 m optical waveguide into the power-over-fiber link, including the isolator showed in Figure 3.3.1, between the laser and the PPC on the other end. The estimated losses for the fiber splices and the connector are 0.01dB and 0.30dB, respectively; the optical fiber attenuation for the first transmission window should also be considered, accounting approximately 0.12dB (forty meters long). Consequently, the total estimated attenuation in the power-over-fiber link is 0.43dB, which does not affect the system operation. Since the system is installed outdoors, according to the international standard IEC 60529, the circuits and optical connectors are allocated inside an IP66 rated enclosure, providing increased long-term functionality and greater protection against dust and humidity. The electronic system placed close to the conductor cable was designed to perform two main functions: provide electrical power to the sensors and data processing elements, carry out the digital-to-analog conversion and the communication between high and low voltage regions. The PPC provides 3.5 V that is raised to 5 V using a DC-DC converter. Another DC-DC converter provides the symmetric  $\pm 10$  V to the Rogowski coil integrator circuit. A low-consumption microcontroller executes data acquisition, treatment and communication between low and high voltage areas. A RMS-to-DC operation is effectuated on the Rogowski coil integrator signal, which produces a sinusoidal function proportional to the current, prior to the microcontroller 10 bit analog-to-digital conversion. The data are serially transmitted at 9600 bps via a 850 nm LED (see Figure 3.3.2). The light signal is coupled to a 40-m-62.5- $\mu\text{m}$  optical fiber, dedicated for data transmission.

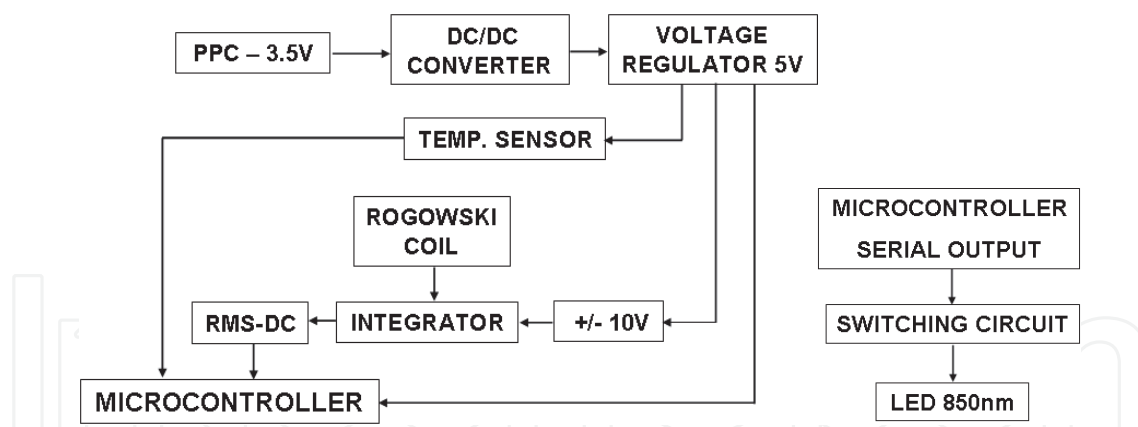


Fig. 3.3.2. High voltage area circuit general view: (Left) microcontroller inputs and voltage levels, (Right) communications schematic.

The low voltage area circuit, located at a base station, performs the optical-to-electrical conversion by a high speed PIN photodiode, operating in photovoltaic mode, using the technique suggested by Werneck and Abrantes [2004]. Before the serial transmission to the instrumentation computer, the signal is converted to EIA-232 levels. Fig. 3.4.1 shows the low voltage area schematic for the monitoring system communications section. Energy to drive the laser for photonic power, which is also situated at the low voltage area, and for the data treatment circuits, after the optical-to-electrical conversion, will be provided by solar energy. Batteries, charged by a solar panel, supply electrical power to the circuits.

### 3.3.4 Conclusions

It has been shown that the proposed monitoring system for transmission line cables measurement of temperature and current provides reliable data. Since silica optical fiber cables are utilized in communications and power supply links, insulation between the sensor head and the user operation site is guaranteed, eliminating the use conventional copper cabling.

The measured values were compared with reference values, the latter being outfitted by commercial measurement laboratory instruments; and small errors were observed, for both current and temperature data. For an even more reliable study of the system accuracy, a calibration using tracked instruments must be carried out.

Future works include the system field installation, in Piracicaba TL, which requires the improvement of system mechanical robustness, and the addition of the sag monitoring subsystem. It is expected that the data collected, together with the sag information, will provide support for the development of an algorithm for the estimation of conductor-sag values.

## 3.4 Optical high voltage sensor based in fiber Bragg grating and PZT piezoelectric ceramics

### 3.4.1 Introduction

Electric power facilities, such as substations, rely on instrument transformers for their functionality and protection. They are divided into voltage transformers (VT) and current transformers (CT) for measuring and controlling voltage and current, respectively. The role of the instrument transformer is to provide accurate signals for protection, control and metering systems, including revenue metering. These requirements place stringent demands on the accuracy and reliability of the instrument transformer to guarantee the correct functionality for protection systems and precise measurement for metering purposes.

Created over a century ago, they are reliable for over-voltage and over-current protection; allow 0.2% revenue metering accuracy and their behavior is well known under both normal and abnormal conditions. Nevertheless, these pieces of equipment are made entirely of copper, ceramic and iron with all empty spaces filled with oil, which are weighty materials, producing bulky, heavy and clumsy equipment. On top of that, they tend to explode without prior warning, resulting in the potential destruction of nearby equipment by pieces of sharp ceramics and furthermore putting the substation personnel at risk.

Optical voltage transducers offer many improvements on traditional inductive and capacitive voltage transformers such as linear performance and wider dynamic range, lighter weight, smaller size and improved safety.

The optical-fiber sensors industry has grown in recent years, and most of the efforts involving the sensors industry focused the use of Fiber Bragg Grating (FBG) as a sensor element. Among the parameters of interest most of the works found in the literature focus on temperature, strain, pressure, displacement, acceleration, vibration, voltage and current.

The behavior of optical current transformer (OCT) and optical voltage transformer (OVT) applied on electric power transmission system has been widely discussed in the literature because they present advantages when compared with conventional transformers. The innovations coming from the optical transformers circumvent problems such as the risk of explosion, high weight, electric safety, insulation oil, difficulty of installation, etc [Sawa et

al, 1990, Cease et al, 1991, Werneck and Abrantes, 2004, and De Nazaré and Werneck, 2010].

However, the main drawback is still the high cost of this new technology, not only for acquisition but also maintenance, demanding specialty skills uncommonly available among company personnel. With this motivation, this case relates the development of a high voltage measuring system to be used as the core of a 13.8-kV-class OVT for the electric power industry application using a PZT (Lead Titanate Zirconate) crystal as voltage transducer and FBG as strain measuring sensor. This new technology can be developed at a cost fully compatible with conventional CTs and VTs.

FBG technology is one of the most popular choices for optical-fiber sensor for strain or temperature measurements due to their simple manufacturing, besides it is relatively easy to deal with and reliable. The use of piezoelectric ceramics in the last decade due to piezoelectric characteristics and transducer properties has attracted interest to electric power systems measurements because of their properties to convert electrical energy to mechanical energy [Niewczas et al, 2005, Yao and Yi, 2006 and Allil and Werneck, 2011].

This study relates to the development of a high voltage sensor system using a PZT piezoelectric crystal as transducer and an FBG as a sensor for an optical voltage transformer for 13.8-kV-class. In the present contribution, a voltage was applied in a combined PZT and FBG sensor by using a high voltage source. This voltage acts on the PZT ceramic causing a mechanical deformation and by using a FBG as interrogation system, the spectrum of the reflected light from the FBG is captured and demodulated to obtain a sinusoidal signal proportional to the applied voltage.

The results showed a linear relationship between the applied voltages to the PZT-FBG sensor with the reflected Bragg wavelength shift. The easy implementation and the low cost of the equipment used prove the viability of this project for applications in the electric power industries.

From previous experimental studies it has been proven that the exposure to ultraviolet radiation during the FBG inscription process decreases the silica yield strength, furthermore, when stretching the FBG to bond it to the stress element, it is necessary to remove the optical fiber coating, and this process can degrade the fiber strength [Miyajima, 1982, Olshansky, Maurer, 1976 and Kurkjian et al, 1989].

To study the mechanical strength and the fiber resistance to strain, in a previous paper [Ribeiro and Werneck, 2010] we measured the tensile strength of silica optical fiber. By providing information about mechanical strength it is possible to obtain a maximum life span for these devices.

### 3.4.2 Experimental setup

As mentioned above, we used a PZT crystal as voltage transducer and a FBG as strain measuring sensor. The experimental setup of the FBG-PZT sensor system is shown in Fig. 3.4.1. The ceramic stack was built using ten 4-mm-thick PZT rings, with  $d_{33} = 300$  pm/V separated by 0.2-mm thick copper electrodes where the contacts were fixed. The electrodes were arranged on both sides of the ceramic discs and were connected in a parallel line. The ceramic disks were glued together separated by the copper plates using EPO-TEK 302-3M resin and kept in the oven for 3 hours at a temperature of 65°C for the cure. A double aluminum structure was used to accommodate the ceramic stack and the 82-mm-length sensor was glued on the top of it.

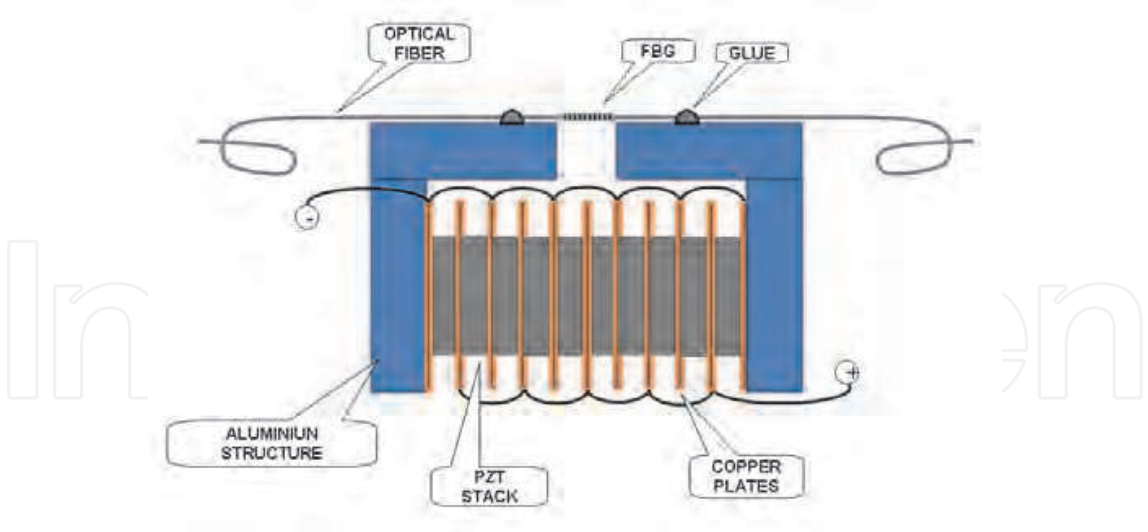


Fig. 3.4.1. Schematic diagram of the FBG-Piezostack.

For improving isolation for high voltage the entire assembly was immersed in a bath of insulating oil. The FBG with central wavelength of 1532.9 nm was stretched to 1535.18 nm as shown in Fig. 3.4.2, before bonded to the aluminum structure to allow measurements in both directions, that is augmenting and retreating PZT thickness.

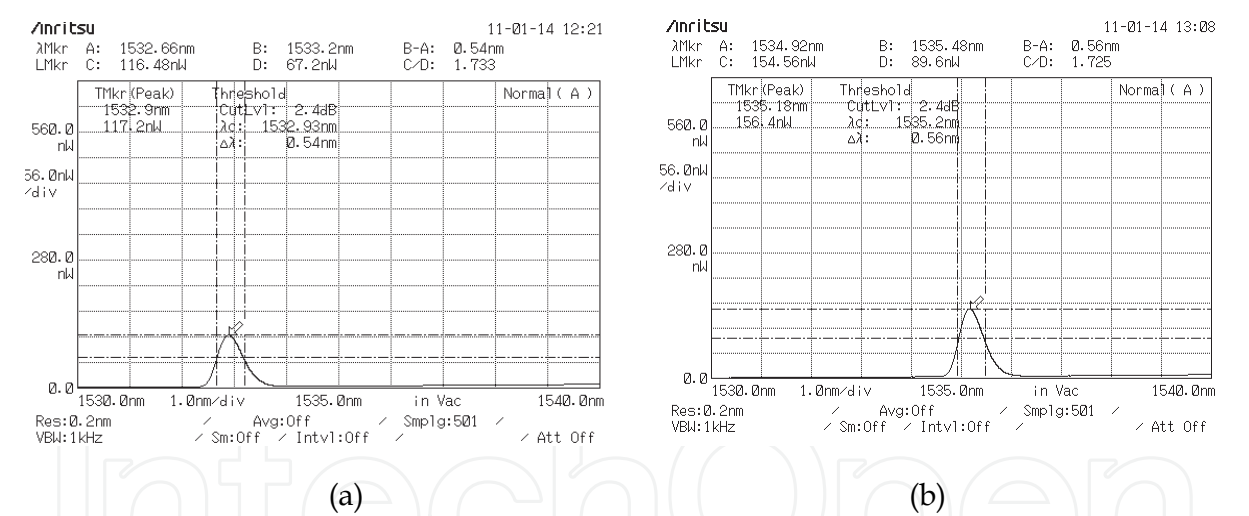


Fig. 3.4.2. (a) The FBG reflection spectrum before bonded to the aluminum base and (b) after bonded.

Notice that by bonding the FBG on the PZT stack as we described, we would have the strain on the FBG equals to the strain on the PZT. This is because, although the total displacement is bigger, so is the length of the fiber, yielding therefore the same strain. Since the fiber is bonded to the ends of the stack, the displacement previewed by (8) will be transmitted to the fiber, so that

$$\Delta L_{PZT} = \Delta L_{FBG}$$

(1)

Now combining (5), (8) e (9) and considering  $\Delta T=0$  (constant temperature environment), we achieve:

$$\Delta\lambda_B=\lambda_B(1-\rho_e) \text{ nd}_{33}V/L$$

(2)

Substituting the PZT constants of Table 3 in (10) we have the following sensitivity for the applied DC voltage:

$$\Delta\lambda_B/\Delta V=128.3 \text{ pm/kV}$$

(3)

Notice that the larger the  $L_{\text{FBG}}$ , the greater the strain experienced by the FBG and consequently, the greater the sensitivity.

Physical and dielectric properties	Value
PZT	
PZT type	PZT4
Ceramic Shape	Ring
Piezoelectric strain constant	$d_{33}=300 \text{ pm/V}$
Thickness of ceramic	$w =4 \text{ mm}$
Maximum allowed direct field strength	$1\text{-}2 \text{ kV/mm}$
Maximum allowed reverse field strength	$350\text{-}500 \text{ V/mm}$
Curie Temperature ( $T_c$ )	$325^{\circ}\text{C}$
Number of elements in stack	$n=10$
FBG	
Bragg wavelength	$\lambda_B = 1535.18 \text{ nm}$
Photo-elastic coefficient	$\rho_e =0.22$
Coefficient of thermal expansion	$\alpha=0.55 \times 10^{-6}/^{\circ}\text{C}$
Thermo-optic coefficient ( $dn/dT$ )	$\eta=8.6 \times 10^{-6}/^{\circ}\text{C}$
Length of FBG	$L=28 \text{ mm}$

Table 3. FBG and PZT Parameters

3.4.3 Optical setup for DC high voltage input

A DC voltage was applied on the PZT crystal terminals by using a high voltage supply and the displacement of the PZT was converted into variations of the Bragg central wavelength. The interrogation system for DC voltage measurements is schematically illustrated in Fig. 3.4.3. The light from an amplified spontaneous emission (ASE) ranging from 1520 nm to 1610 nm was used to illuminate the sensor and a commercial interrogation system from FOS&S model Spectral Eye 400, with accuracy of 2.0 pm was used to measure the reflected FBG spectrum accordingly to the sensor displacement.

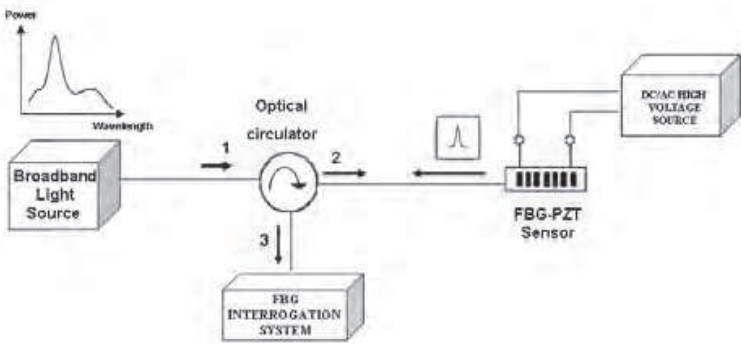


Fig. 3.4.3. Schematic diagram of experiment setup for DC voltage.



For the first experiment, only DC voltages were applied to the PZT in order to measure the Bragg displacement accurately by the interrogation system. Eq. 9 was used to calculate the maximum voltage to be applied to the PZT ceramic and do not exceed the allowed value, accordingly with the Table 3.

$$V = E.d_{ij}$$

(4)

By applying a DC voltage to the PZT and recording the respective Bragg shift we can see the linear relationship between the applied voltage and the central Bragg wavelength (Fig. 3.4.4). The results show that the measured sensitivity was of 91.5 pm/kV and the correlation coefficient (R2) were 0.999.

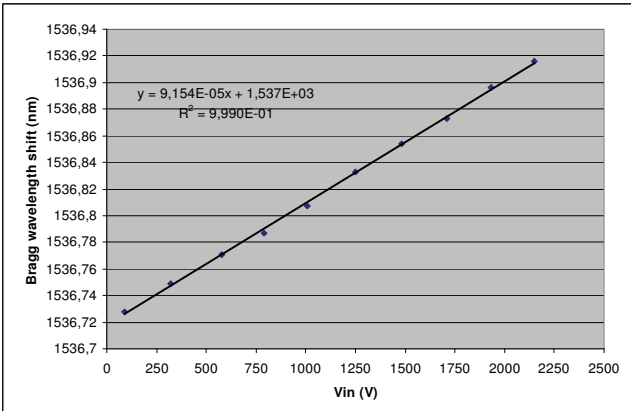


Fig. 3.4.4. FBG-PZT sensor curve when a DC voltage is applied

3.4.4 The optical setup with a AC voltage power supply

Fig. 3.4.5 represents the interrogation system for AC voltage measurements. Since the optical spectrum analyzer is too slow to respond to the 60-Hz line frequency, the central wavelength variation can be obtained by using a photo-detector. The light from the ASE illuminates the FBG-PZT sensor via an optical circulator. The reflected spectrum of the sensor pass through the Fabry-Perot tunable filter (FFP-TF) with 0.89 nm bandwidth, nominal finesse of 130 and 116 nm of free spectral range (FSR). The light signal enters an amplified photo-detector with designed for detection of light signal over 700 nm – 1800 nm. The AC output signal is monitored by an oscilloscope. The FFP filter was tuned in 1540.04 nm by applying a voltage of the 7.2 volts. This point indicates that the FFP filter is matched with the FBG sensor on the stack and the intensity of light at the photo-detector is at maximum.

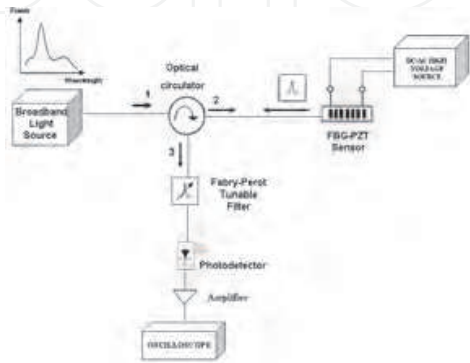


Fig 3.4.5. Schematic diagram of experiment setup for AC voltage.

From Fig. 3.4.6 we can see a linear relationship between the AC voltage applied to the FBG-PZT sensor and the output signal. A high voltage source was used to supply the input signal ranging from 0 kV to 2 kV at the terminals of the PZT electrodes, and on Figure 3.4.7 we can see the sequence of screens of the oscilloscope when an increment of AC voltage is applied to the PZT terminals.

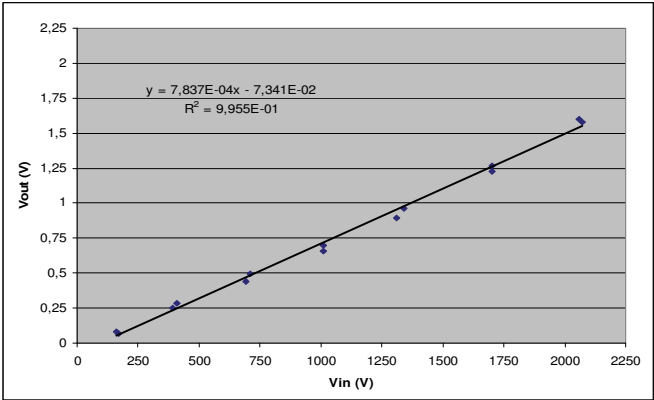


Fig. 3.4.6. Relationship between the input AC voltage versus output signal

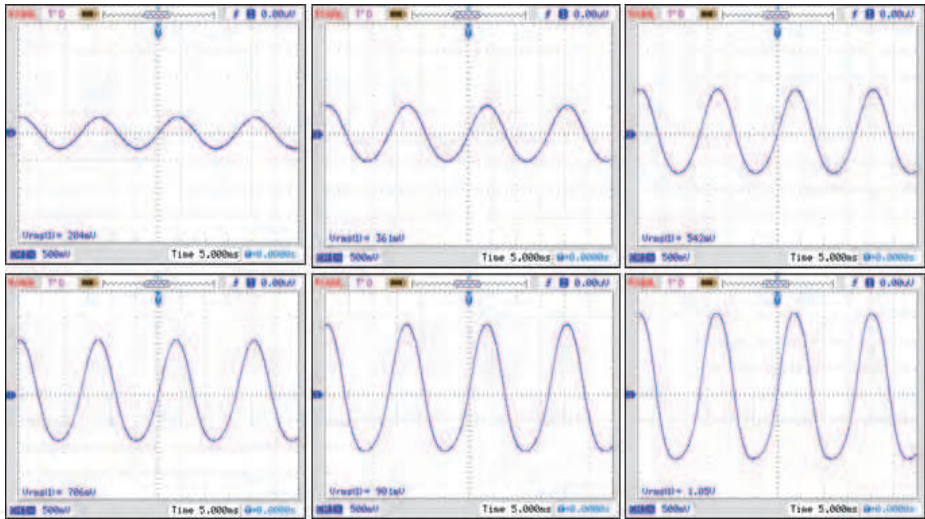


Fig. 3.4.7. Photodetector output signal for each increment of the AC voltage applied (V<sub>rms</sub>)

3.4.5 Mechanical and temperature stability

All mechanicals parts are very rigid, including the PZT ceramics and the FBG itself which presents a Young modulus of 70 GPa, close to that of steel as measured in section II. In an OVT the vibrations are mainly of 60 Hz, due to magnetic movement of the transformer core. However, in the case of an optical CT, there is no iron core to vibrate and then this equipment is noiseless and does not present this kind the vibrations. Figure 3.4.8 shows the results for several acquisitions employing the sensor, where a low dispersion of results when a DC voltage is applied on the terminals of the sensor can be observed. However, it is important to notice that one degree Celsius in temperature change will cause an approximately 14 pm Bragg wavelength displacement. Therefore, temperature compensation is important in DC/AC applications because the drift caused by temperature

variation will affect not only the sensor response, but also all parts of the transducer, producing unwanted drifts. However for DC only, a simple high-pass filter easily filters out temperature drifts from the output signal. A picture of the sensor on the high voltage rig is shown in Fig. 3.4.9.

This experiment provided information for the mathematical model developed in section IV and showed a good repeatability in sets of measurements and a correlation coefficient  $R^2=0,997$ .

IntechOpen

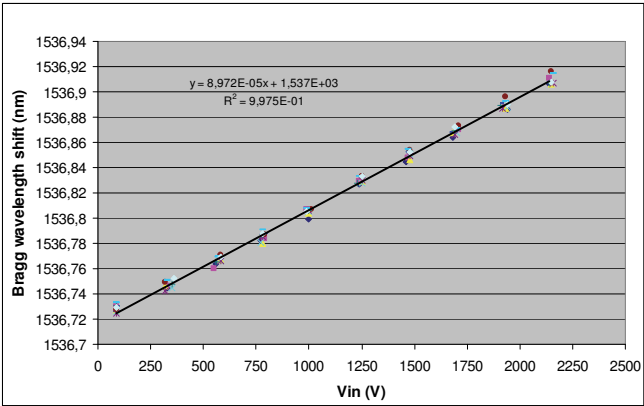


Fig. 3.4.8. FBG-PZT sensor curve when a DC voltage is applied

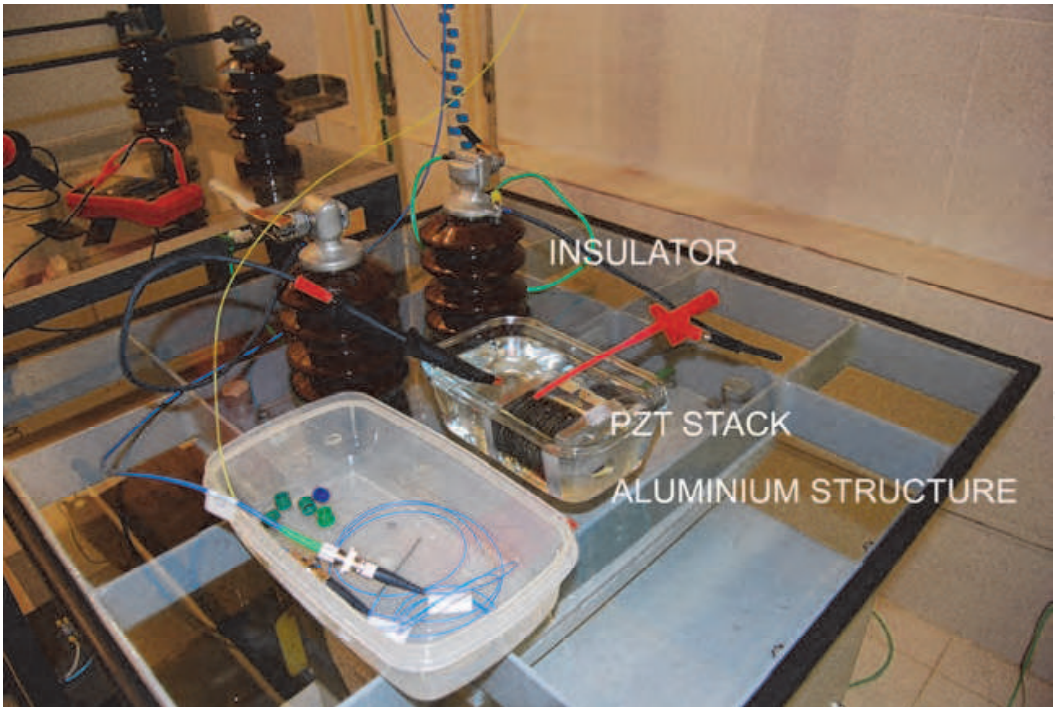


Fig. 3.4.9. Photograph of the FBG-PZT sensor.

### 3.4.6 Conclusions

In this work, it was presented the development of an optical high voltage transformer based in FBG and PZT piezoelectric ceramics for use on a 13.8 kV-Class electric power

transmission system. The advantages of piezoelectric material with the characteristics of a sensor fiber Bragg grating is employed. For the assembly of the prototype used, the aluminum structure was designed in order to support a larger number of ceramic rings and thus increase the longitudinal displacement of the material by improving the resolution of the demodulation system. An aspect to be considered is related to the maximum field strength allowed according to the manufacturer's specifications restricting the voltage applied to the sensor, an aspect that can be solved with a capacitive divider. Despite this limitation, the results make it viable the use of this technology for monitoring power substations. In order to improve the system and increase accuracy, a more appropriate setup is under development. An increased longitudinal displacement can be obtained with a new prototype sensor based on ceramics with a higher piezoelectric charge constant and by encapsulation of the sensor by increasing the sensitivity.

### **3.5 Fiber Bragg grating temperature sensor system applied to large air cooled hydrogenerators**

#### **3.5.1 Introduction**

This project describes the research, project, construction, calibration, installation and operation of a fiber Bragg grating based fiber-optic system applied to a hydro-electric generator to perform a continuous monitoring of temperature. After being deployed for two and a half years, the system has proved itself to be capable of reliably and accurately measuring and monitoring temperatures inside the generator, even taking into consideration the harsh environment of the stator. The results were considered satisfactory, demonstrating the usefulness of the fiber-optic system in power generation equipment.

The technology of power generation by hydro-electric plants (HEP) in Brazil has reached a high level of sophistication and investment. Nowadays about 73% of all electric energy produced in the country is from HEPs, including very large ones such as Itaipu and Tucuruí with 14 and 8.3 GW respectively. This figure will increase further with the already in construction Rio Madeira Complex whose 88 turbines will produce over 6.8 GW and Belo Monte (11.3 GW) in licensing processes.

This electric grid represents a very high capital invested which is also of very expensive maintenance. Each minute down time of any piece of equipment could cost the energy providers thousands of dollars from profit losses of undelivered energy and also from several types of fines applied by the National Electric Power Agency which they are subjected to.

For this reason the reliability of equipment has become a highest priority and many control systems have been designed to protect and perform real time diagnosing for prompt shutdown or warnings in case of faults.

The main control parameter in any HEP or substation is, of course, the electric current that can rise without limits in case a short-circuit or excess load occurs. The second parameter in importance is the voltage that may present surges or transients due to switching or atmospheric discharges. The third parameter, normally a consequence of the current, is the temperature that must be under severe observation since rises above 100°C can accelerate aging of the insulating material and conductors or even destroy them, causing a general



failure of the generators or transformers. Paradoxically, since current and voltage maintain their values approximately the same all over the HEP, there are much more temperature control points in a HEP than there are for current or voltage.

With the idea of decreasing the amount of copper wires, facilitating the maintenance, possibility of remote sensing and consequently decreasing costs, we designed a fiber-optic multiplexed temperature sensor for application in large air cooled HEP. The system has the objective to cover all temperature monitoring needs of a HEP that would also overcome some the disadvantages presented by the conventional RTD (resistive temperature detector) network.

The Eletronorte, the largest electric energy producer in Brazil, contracted the Instrumentation and Photonics Laboratory, at the Federal University of Rio de Janeiro to project, test and install a complete FBG system to monitor the temperatures inside hydro-generator.

This paper relates the world's first real application, test and operation of a FBG temperature sensor array inside a fully operational and connected-to-the-grid hydro-electric power generator.

### 3.5.2 Hydrogenerator temperature monitoring

Although hydro-generators are very reliable, the temperature monitoring of these machines is a well-established procedure. The reason for this is that the stator windings, cooper and insulation, age over time and tend to degrade when the machine operates at relatively high temperatures such as the in the range 100-120°C [Stone, G. C., 1999]. Keeping the temperature below these limits is not easy because large hydrogenerators stators and rotor can weigh as much as 1,000 tons and 1,700 tons, respectively, and as a consequence, these machines have a big thermal time constant.

For keeping the temperature below these limits, large hydro-electric machines of 40 MW or more are normally air cooled. These generators are supplied with a closed air-cooling circuit where the air is cooled by a water refrigerated radiator. In this type of generator the air temperature is monitored before and after it passes through the radiators.

The temperature monitoring of the cooling air or directly inside the stator winding conductors are the most reliable methods of assuring the proper operation of power generator [Stone, G. C., 1999] and for these measurements, the most popular sensor is the Pt-100, meaning 100  $\Omega$  platinum resistance sensor, also known as RTD. These sensors are placed at various locations within the generator, for instance, in the cooling air passages, inside the lubricant and hydraulic oil pipes, in the bearings and also inserted into the slots of the stator core, summing up to about fifteen or more sensors for each machine.

These reliable, accurate and relatively inexpensive sensors are in use by the industry for almost a century and perfectly fulfill all temperature monitoring needs of a HEP. They have disadvantages, though, that can be mentioned: a) sensitivity to electromagnetic interference (EMI), demanding low pass filters; b) tendency to carry the high voltage of the generator to the control room if short circuits occur; c) tendency to burn inside the slots of the stator winding where they cannot be replaced. Additionally, each sensor is driven by a three wire harness that needs to go all the way from the machine to the control room where a large rack with many modules receives each sensor harness. For larger distances it is necessary to



use a current loop to carry the information signals, therefore a terminal box must be installed close to the sensor location with amplifiers, filters and converters to 4-to-20 mA, for example. In a relatively large HEP with ten generators, there are many terminal boxes, harnesses, plug-in modules and racks all over the plant with hundreds of kilometers of electric wires. This is the principal aspect where a multiplexed sensor array can help, as with only a few fiber-optic cables the system can manage all temperature check points of the whole plant.

The feasibility of application FBG sensors in electric machines for temperature monitoring has been the theme of many recent works. One of them is the paper from a Siemens AG engineer team [Theune, et al., 2002] in which the authors investigate the application of FBG sensors embedded into the stator core of a generator on a test bench. This test demonstrated the viability of the FBG technique applied to generators. More recently, the internal temperatures of oil-immersed power transformers were measured by FBG arrays extending the application of this kind of fiber-optic sensor in electric machines [Kim et al., 2008, Weigen et al, 2008 and Ribeiro et al, 2008]

### 3.5.3 FBG theory

Fiber Bragg Grating (FBG) technology is one of the most popular choices for optical fiber sensors for strain or temperature measurements due to their simple manufacture (UV photo-inscribed) and relatively strong reflected signal strength. They are formed by a periodic modulation of the index of refraction of the fiber core along the longitudinal direction and can be produced by various techniques [Othonos and Kalli, 1999 and Meltz et al., 1989].

Since the strain or temperature measurands are encoded into wavelength shifts, these sensors are also self-calibrated because wavelength is an absolute parameter. Thus these sensors do not drift on the total light levels, losses in the connecting fibers and couplers or light source power. Additionally, the wavelength encoded nature of the output also allows the use of wavelength division multiplexing technique (WDM) by assigning each sensor to a different wavelength range of the available light source spectrum.

In the FBG, due to the periodic modulation of the index of refraction, light guided along the core of the fiber will be weakly backwards reflected by each grating plane. The contribution of the reflected light from each grating plane will add up with each other in the backward direction. This addition can be constructive or destructive, depending on whether the wavelength of the incoming light satisfies or not the Bragg condition, given by:

$$\lambda_B = 2n_{eff} \cdot \Lambda \quad (1)$$

Where,  $n_{eff}$  is the effective index of refraction of the fiber core and  $\Lambda$  is the modulation period of the index of refraction.

Equation (1), also known as the Bragg reflection wavelength, is the peak wavelength of the narrowband spectral component reflected by each FBG of the array. The FWHM (full-width-half-maximum) or bandwidth of this reflection depends on several parameters, particularly the grating length. Typically, the FWHM is 0.05 to 0.3 nm in most sensor applications. Equation 30 also shows that the Bragg wavelength is a function of  $\Lambda$  and  $n_{eff}$ . Thus we conclude that a longitudinal deformation due to an external force can change both  $\Lambda$  and  $n_{eff}$ , the later by the photo-elastic effect and the former by increasing the pitch of the grating.

Equivalently, a variation of temperature can also change both parameters, by thermal dilation and by the thermo-optic effect respectively.

With such a device, by injecting a spectrally broadband source of light into the fiber, a narrowband spectral component at the Bragg wavelength will be reflected by the grating. In the transmitted light, this spectral component will be missed but the remaining of this light can be used to illuminate other FBGs in the same fiber, each one tuned in a different wavelength. The final result of such arrangement is that we will have at the beginning of the fiber all Bragg peak reflections of each FBG, each one in its specific wavelength range.

Now, by designing the proper interface, measurands can be made to impinge perturbation on the grating resulting in a shift in the Bragg wavelength which can then be used as a parameter transducer.

Starting from the theorem of the conservation of energy and momentum, after a series of algebraic manipulations, very well detailed in [Othonos and Kalli, 1999], one arrives to the following equation, which establishes the relationship between the Bragg wavelength, strain and temperature applied to the FBG:

$$\frac{\Delta\lambda_B}{\lambda_B} = (1 - \rho_e)\varepsilon_z + (\alpha + \eta)\Delta T \quad (2)$$

Where,  $\varepsilon_z$  is the longitudinal strain;  $\Delta T$  is the temperature variation;  $\rho_e$  is the photo-elastic coefficient;  $\alpha$  is the thermal expansion coefficient and  $\eta$  is the thermo-optic coefficient, representing the temperature dependence of the refractive index ( $dn/dT$ ). For materials with positive thermal expansion coefficient, the index of refraction normally decreases with temperature. These parameters have the following values for a silica fiber with a germanium doped core:

$$\begin{aligned} \rho_e &= 0.22; \\ \alpha &= 0.55 \times 10^{-6}/^{\circ}\text{C}; \\ \text{and } \eta &= 8.6 \times 10^{-6}/^{\circ}\text{C}. \end{aligned}$$

Since we want to measure only the temperature, we must protect the fiber against strain by placing the grating portion of the fiber inside a protective tubing, for instance. Thus the sensitivity of the grating for temperature at the wavelength range of 1550 nm is, after substituting the constants in (2):

$$\frac{\Delta\lambda_B}{\Delta T} = 14.18 \frac{\text{pm}}{^{\circ}\text{C}} \quad (3)$$

This theoretical value, though, is not absolute as each FBG of the same fabrication batch will present slightly different sensitivities, as we will see later in the following sections.

### 3.5.4 Calibration of sensors

Before installing the sensors into the generator they had to be calibrated because, as already mentioned, (3) is not valid for all FBGs as they may have different thermo-optic coefficients and they are tuned into different wavelengths.

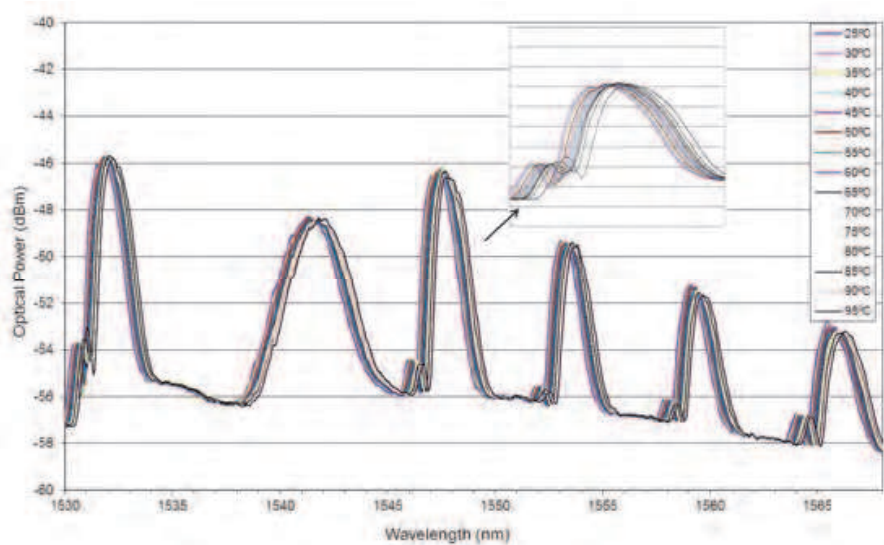


Fig. 3.5.1. Superimposed wavelength shift of each FBG as temperature varies from 25°C to 95°C.

The calibration procedure of the sensors followed two steps. In the first set of measurements, the six sensors were calibrated simultaneously by immersion into a temperature controlled bath and the Bragg wavelengths were monitored along with the temperature in order to calculate the sensitivity of each sensor, as predicted by (3). This first set of measurements allowed us to observe and measure the Bragg shift of each FBG as a function of temperature in the range of 25°C to 95°C. Fig. 3.5.1 shows all Bragg reflection of each temperature superimposed. In this experiment it is important to make sure that each pulse does not enter the neighbor’s range during its displacement. From this data the software calculates the center wavelength of each Bragg reflection and plots the Bragg shift versus temperature for each FBG, producing the graph shown in Fig. 3.5.2.

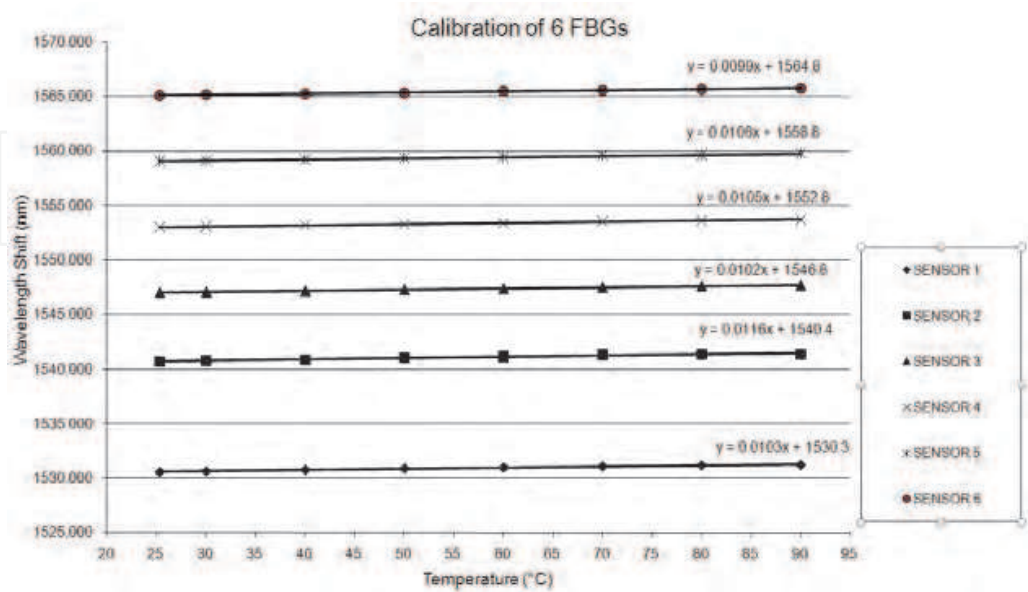


Fig. 3.5.2. Wavelength shift versus Temperature for each FBG.

Table 4 summarizes the information acquired from the last experiment.

Sensor #	Theoretical Sensitivity (pm/°C)	Measured Sensitivity (pm/°C)	Wavelength @ 25°C (nm)
1	14.00	10.3	1530,534
2	14.10	11.6	1540,667
3	14.16	10.2	1547,027
4	14.21	10.5	1553,035
5	14.27	10.6	1559,063
6	14.32	9.9	1565,090

Table 4. Theoretical and measured sensitivities of each FBG.

Notice in Table 4 that, as predicted by (3), the theoretical sensitivities are different from those obtained in the calibration experiment. But, since all FBGs were made out of the same optical-fiber reel,  $\alpha$ , the silica coefficient of temperature should be the same for all FBGs produced from that fiber. The other parameter in (3) is  $\eta$ , the thermo-optic coefficient, representing the temperature dependence of the refractive index ( $dn/dT$ ). Equation (1) teaches us that  $\lambda_B$  is a function of  $n_{eff}$ , the average index of refraction between the pristine fiber core and that of the ultra-violet-irradiated core. Recall that during the FBG fabrication, the radiation time for each FBG inscription is not the same as the operator turns off the laser only when she observes the Bragg reflection above a certain level. Since the UV irradiation modifies the index of refraction of the fiber core, it is possible that it could also modify differently the values of  $\eta$  in each FBG, ending up to the slightly dispersed sensitivities found above. However, to the best of our knowledge, there is no mention of this effect whatsoever in the literature.

The data obtained from Fig. 3.29 also allow us to calculate the linear relationship between wavelength and temperature for each FBG. These equations were fed into the software in order to calculate the temperature of each sensor.

The second step of the calibration procedure was the comparison between the calculated temperatures by the optical interrogator software with the calibrated temperatures of each FBG, as given by a precision thermometer. From this experiment it was possible to calculate the inaccuracy of the measurement which was less than 0.5°C, quite sufficient for this application. The correlation coefficient of the linear curve fitting was 0.9994 as shown in Fig. 3.5.3.

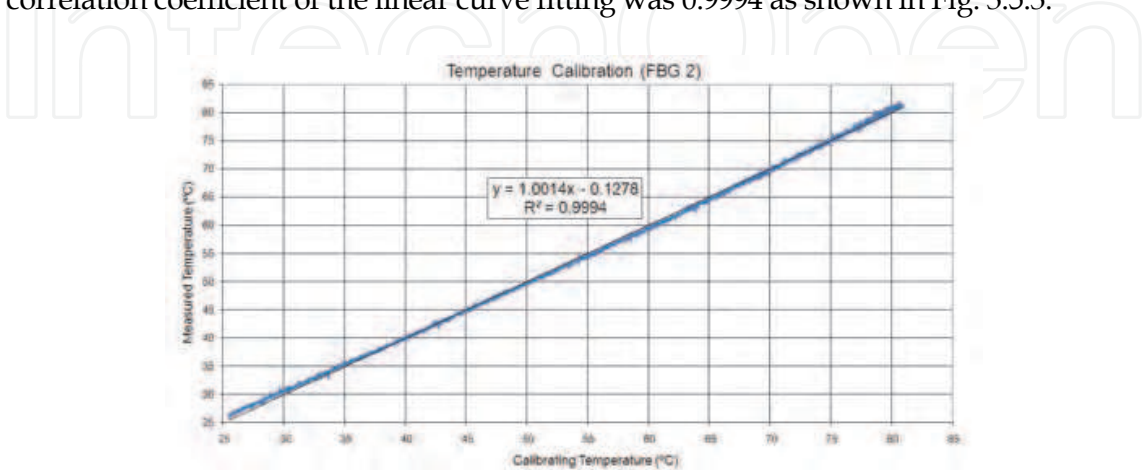


Fig. 3.5.3. Calibration of FBG 2.



### 3.5.5 Installation of sensors and results

The HEP chosen for this experiment was the UHE-Samuel, at Brazil's far west city of Porto Velho, close to the border with Bolivia. UHE-Samuel is located at the Jamari River, a tributary of the Madeira River, which in turn, is one of the major tributaries of the Amazon River. The UHE-Samuel generates 216 MW and counts with five Kaplan-type turbines generating each one about 42 MW.

The system began to be installed in the generator number five in November 2007. This process was performed in two opportunities: during a five-day shutdown of the machine for maintenance and in another five-day window for retrofit (exchange of rectifiers).

For the installation of the sensors inside the stator it is obviously necessary to turn off the machine, which is not an easy task. This is because, as the majority of HEPs in Brazil, UHE-Samuel is a national-grid-connected HEP therefore to be turned off, one needs a special authorization issued by the National System Operator. The request is normally dispatched six months in advance, and if granted, the machine is allowed to be turned off during a five-day window.

The machine, which operates at a normal temperature around 95°C, needs 24 hours to drop its temperature to about 45°C in order to be possible to enter inside the stator hall to install the sensors. The stator environment can be considered to be one of the worst places a sensor can be installed in. Its average temperature is about 95°C peaking up to 110°C with an air humidity close to 100%; it presents a dense oily atmosphere; a very high electro-magnetic interference at a few millimeters from 15 kV conductors carrying a current of 2 kA; vibrations of every kind up to 0.3 G and among heavy parts that are frequently assembled and disassembled using heavy tools with huge force. How can so a fragile sensor, such as a 125- $\mu\text{m}$ -diameter-glass-optical-fiber-sensor, be installed in such harsh environment and even though keep its reliability during the expected 40-years life span?

A FBG used as a temperature sensor presents a very small time constant because it has a small mass. In order to protect this sensor and do not deteriorate such a valuable parameter the sensor was installed loosely inside a thin U-form copper tubing in order to allow a good heat transfer between the cooling air and the optical fiber, as shown in Fig. 3.5.4. The tubing, which also protects the fiber against strain, goes out and back again from an IP65 polymeric enclosure.



Fig. 3.5.4. Box containing the fiber-optic splices with the FBG inside the U-shape copper tubing (left) and installed inside the generator (right).

An adequate fiber-optic cable connected all six boxes as they were installed around the stator winding behind of each radiator of the generator. The optical cable was then placed

within the existing cable trays along with other electric cables following all the way up, from the generator to the HEP control room where the optical interrogator and an industrial PC were installed.

The optical interrogation setup consists of a broad band optical source that illuminates all FBGs in the array. The return signal of each FBG is detected by an optical spectrum analyzer (OSA) that identifies the center wavelength of each FBG reflection pulse. The OSA communicates with an industrial PC via RS-232 interface, running a LabView software for calculation and storage of the temperatures. The PC publishes all data into the company's Intranet that automatically and instantaneously become available to the HEP central software control. Fig. 3.5.5 shows the block diagram of the system.

However, the proposed system goes much further in ambition. After the approval of the current system, the proposed project planes to use this technology to fulfill all temperature needs of the HEP, including turbines, air, oil and water ducts and other electrical equipment as well at the substation (see Fig. 3.5.6). Since a single optical fiber cable can monitor about 16 or more sensors, it is just necessary one cable per equipment for all temperature measurements. The system is also intended to access the Internet so as to be able to be accessed remotely, even from another location. This is especially advantageous for automatic unmanned substations.

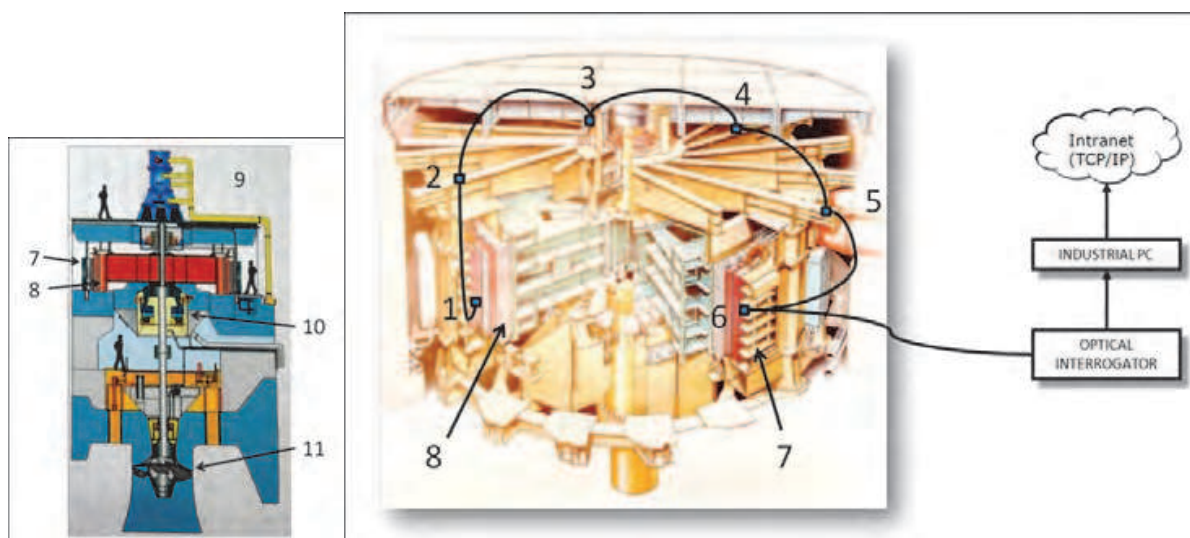


Fig. 3.5.5. Depiction of a cross-section of the hydro-generator (left). Generator in detail with sensors connected to the interrogation system (right). 1 to 6) FBG sensors; 7) Radiator; 8) Stator; 9) Machine room; 10) Bearing; 11) Kaplan turbine.

Shortly after the installation we noticed that the last two FBGs in the fiber-optic cable were not identified by the optical interrogator, probably due a malfunction of the optical connectors. But there was no time to open up again the inspection windows of the stator as the machine was programmed to start up immediately. Since then, the machine did not stop again as our requests for shutting down were not granted so far. Currently, at the time of writing this article, the machine is in operation for two and a half years and the fiber-optic system is monitoring normally four radiators. The results of the measurements are sent periodically to the company's head-quarters in Belém, some 1,800 km north and from there to our laboratory located in Rio de Janeiro, 2,400 km south.

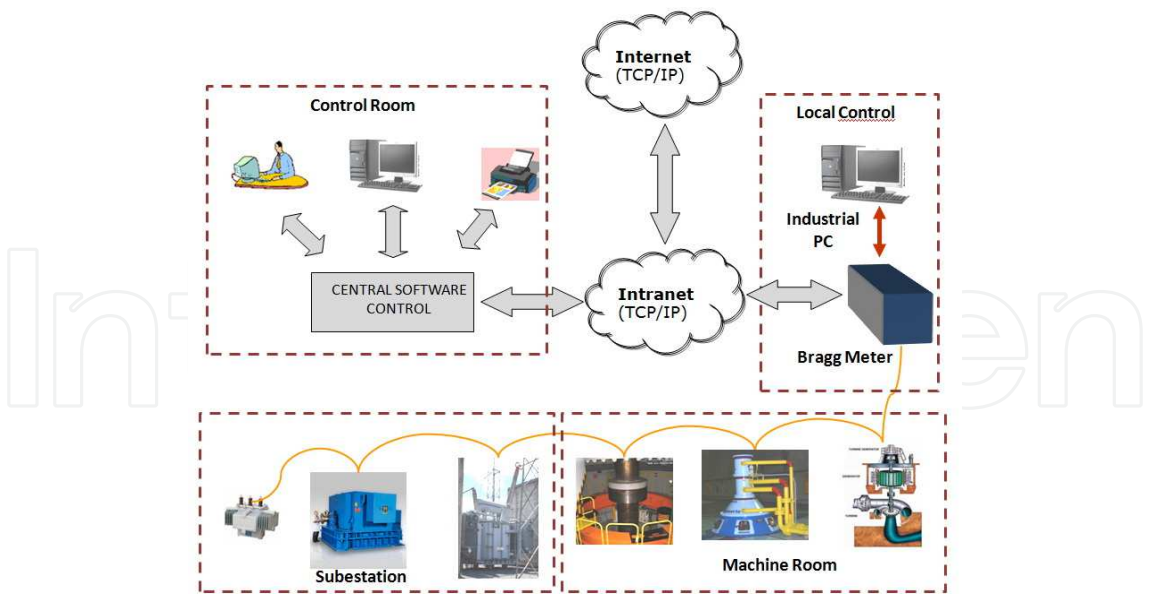


Fig. 3.5.6. Proposed extension of the system including all monitoring needs of the hydro-electric plant.

Just after the installation the system started the monitoring the temperatures, producing the graph shown in Fig. 3.5.7. We can observe all signals superimposed at about 33°C.

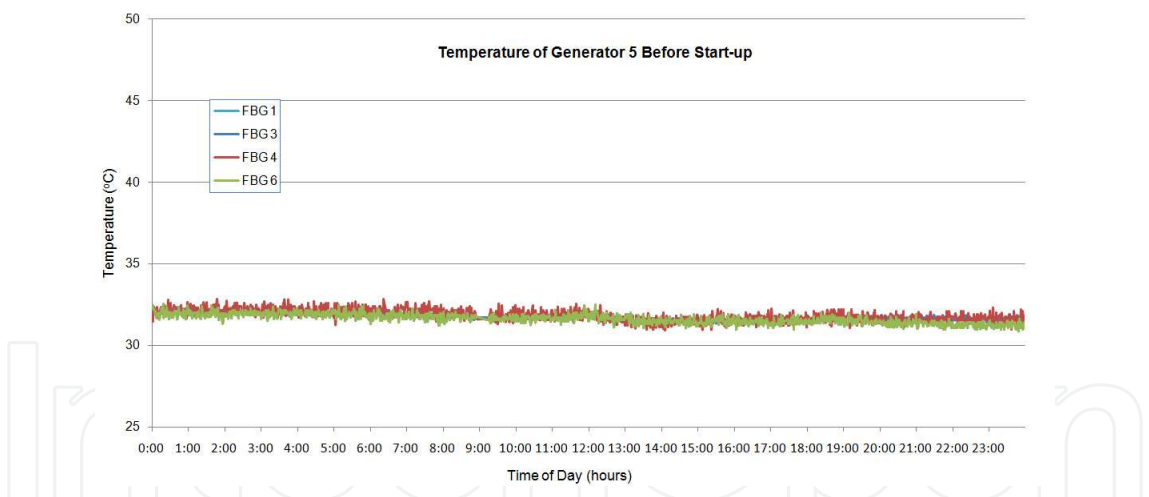


Fig. 3.5.7. Temperature of generator 5 before start up.

After the installation the machine was several times started up and down in test procedures. The graph in Fig. .45 shows the evolution of the temperature during the last start up test of the generator. Notice that, differently than in Figure 3.5.8, the temperatures of the radiators were not the same before start up. This is because the machine was working before with different temperatures around the stator, which is normal as it will be seen later. At 9 AM the turbine was opened to the dam and the machine started-up. The temperature at FBG 3 rose from around 35°C to 85°C while the turbine accelerated up to 90 rpm until in phase with the 60 Hz grid frequency. Then, at 6 PM the generator was switched to the national grid and the temperature rose again up to 95°C, stabilizing thereafter.

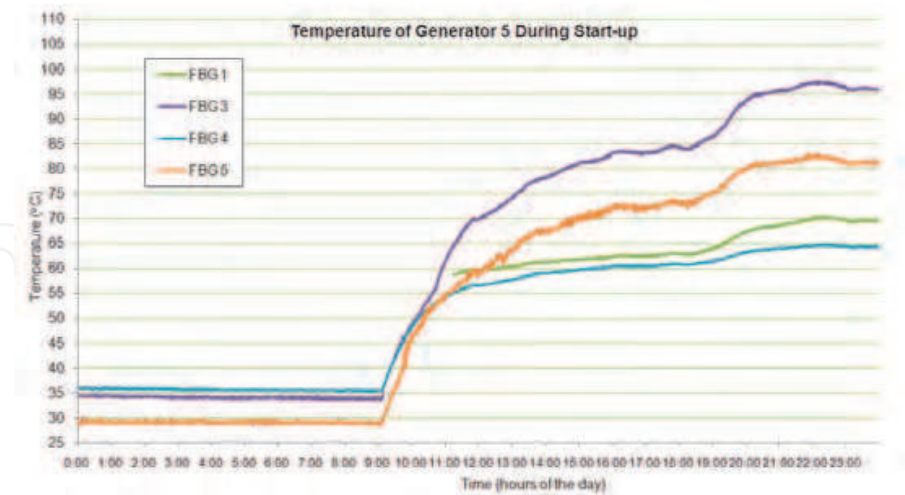


Fig. 3.5.8. Temperature evolution of generator 5 during start up.

Fig. 3.5.9 shows the temperature of the generator in normal operation. At this time the generator was producing 22 MW with an average water flow of 82 m³/s.

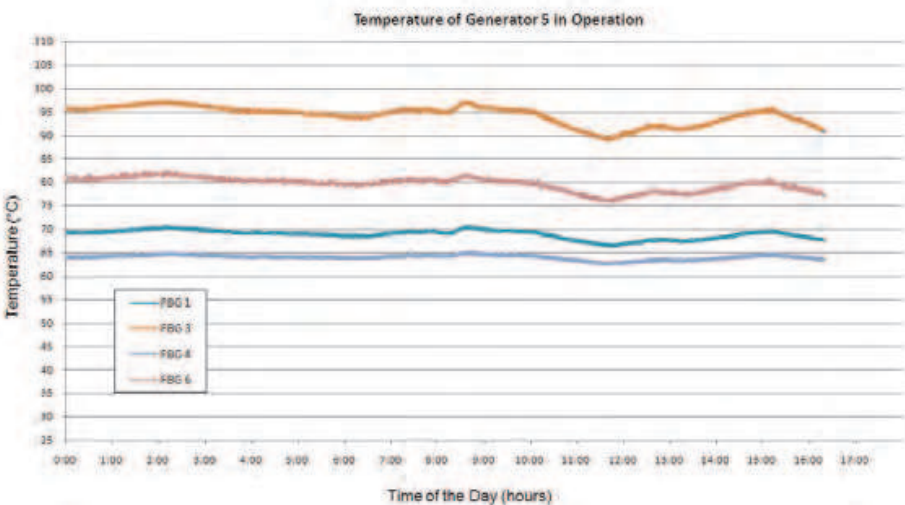


Fig. 3.5.9. Temperature of generator 5 in operation.

As in Fig. 3.5.8, we can still observe in Fig. 3.5.9 a difference in temperature between different sections of the generator. For explaining this behavior it is necessary first to understand how the cooling system works. The cold water from the bottom of the dam is taken by a pipe and, after a chlorine treatment, it feeds the radiators, one after the other, in a row. But as the water pipe goes around the stator feeding each radiator, the water loses pressure so that the first radiator has a higher water flow than the second, and so on until the water reaches the last radiator which receives much less water. Therefore, each section of the stator is cooled down to different temperatures leading to the behavior observed in Fig. 3.5.8 and Fig. 3.5.9. Of course a load unbalance between the phases would also lead to different temperatures but in a 5-machine plant with all generators interconnected this would be very difficult to happen.



Observing Fig. 3.5.9 it is possible to notice that, even in steady state the generator temperatures vary along the time, with all temperatures following the same pattern. This is how the generator responds to the energy demands by the load.

### 3.5.6 Conclusions

This case described the world's first real application, test and operation of a FBG temperature sensor array inside a fully operational and connected-to-the-grid hydro-electric power generator. The FBGs sensors were installed inside the generator in November 2007 and are in continuous operation since then. The system was capable to measure and monitor reliably and accurately temperatures inside the generator even considering the harsh environment of the stator generator.

With this system in operation a large reduction of installation and maintenance costs could be avoided since many kilometers of electric wire would be saved.

Another conclusion of such experiment is that it is very difficult to conciliate research and commercial interests. Scientists working with power generation find enormous difficulties in having machines turned off, particularly those connected to the national grid. Power operation authorities are so much concerned about system reliability and energy production without discontinuities that often refuse any kind of research proposals that could, in any way, put in jeopardy machines integrity or interrupt energy production.

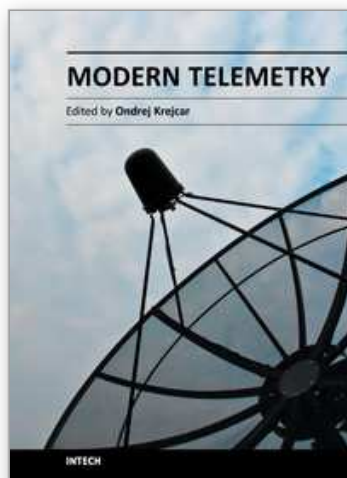
## 4. References

- R. C. S. B. Allil and M. M. Werneck, "Optical High Voltage Sensor based in Fiber Bragg Grating and PZT Piezoelectric Ceramics", *IEEE Transactions on Instrumentation and Measurement*, Vol. 60, Issue 7, 2011
- K. Asada and H. Yuki, "Fiber optic temperature sensor", 3<sup>rd</sup> POF'94, p. 49-51, Yokohama, Japan (1994).
- J. B. Briggs, "Leakage current monitoring system and method", U.S. Patent 3,947,759 (1976).
- G. Böttger, M. Dreschmann, C. Klamouris, M. Hübner, M. Röger, A. W. Bett, T. Kueng, J. Becker, W. Freude and J. Leuthold, "An optically powered video camera link", *IEEE Photonic Tech. Letters*, vol. 20, no.1, pp. 39-41, Jan. 2008.
- T. W. Cease, J. G. Driggans, and S. J. Weikel, "Optical voltage and current sensors used in a revenue metering system", *IEEE Transactions on Power Delivery* Vol. 6, Issue 4, pp. 1374-1379, October 1991.
- D. A. Douglas and R. Thrash, "Sag and tension of Conductor - The Electric Power Engineering Handbook", CRC Press/IEEE Press. 2007.
- S. Tumanski, "Induction coil sensors-a review", *Measurement Science and Technology*, vol. 18, no. 3, R31-R46, March 2007.
- F. Amarh, "Electric transmission line flashover prediction system", PhD Thesis, Arizona State University, May (2001).
- K. T. V. Grattan and Z. Y. Zhang, "Fiber Optic Fluorescence Thermometry", Chapman & Hall, London (1995).
- R. W. Hertzberg, *Deformation and Fracture Mechanics of Engineering Materials*, Wiley; 4<sup>rd</sup> edition, Chapter 4, December 1995.
- IEC 60793-1-1 "Optical fibres - Part 1-1: Measurement methods and test procedures - General and guidance", International Electrotechnical Commission, 2008.

- A. D. Kersey, M. A. Davis, et al. "Fiber grating sensors. *Journal of Lighthwave Technology*," N°8, 1997, pp. 1442-1463.
- B. Jaffe, R. S. Roth, and S. Marzullo, "Piezoeletric porperties of lead zirconate-lead titanate solid-solution ceramics", *J.Appl.Phys.*, vol.25, pp. 809-810; June, 1954.
- A. G. Kanashiro e G. F. Burani, "Leakage Current Monitoring of Insulators Exposed to Marine and Industrial Pollution", *IEEE International Symposium on Electrical Insulation*, 271-274, Quebec, Canada, (1996).
- C. R. Kurkjian, J. T. Krause, M. J. Matthewson, "Strength and Fatigue of Silica Optical Fibers", *Journal of Light Techonology*, pp: 1360-1370, Vol.7, N° 9, September 1989.
- R. A. Maraio, A. T. McMahon and H. B. Hart Jr., "Method and detector for identifying insulator flashover", U. S. Patent 5,136,248 (1992).
- D. A. Ward and J. L. T. Exon, "Using Rogowski coils for transient current measurements", *Eng. Sci. Education J.*, vol. 2, pp. 105-113, 1993.
- J. Marcou (editor), "Plastic Optical Fibers: Practical Applications", Club des FibresOptiquesPlastiques, Wiley & Sons, France (1997).
- B. Culshaw& J. Dakin (editors), *Optical Fiber Sensor*, Artech House, London, 1989 and 1997.
- J. N. Mitchell, "Limits of electrical power generation by transmission of light through optical fibers", *Applied Physics Division – Southwest Research Institute*, 2004, San Antonio, USA.
- M. R. Spiegel, "Statistics", McGraw-Hill of Brazil, Rio de Janeiro, 1971.
- Y. Miyajima, "Studies on High-Tensile Proof Tests of Optical Fibers", *Journal of Lighthwave Techonology*, pp. 340-346, Vol. LT-1, N° 2, June 1983
- De Nazaré, F. V. B., Weneck, M.M., "Development of a monitoring system to improve ampacity in 138kV transmission lines using photonic technology", *IEEE Transmission and Distribution Conference and Exposition*, 2010, pp.1-6.
- P. Niewczas, L. Dziuda, G. Fusiek, and J. R. Mc Donald, "Design and Evaluation of a Preprototype Hybrid Fiber-Optic Voltage Sensor for Remotely Interrogated Condition Monitoring System", *IEEE Transactions on Instrumentaion and Measurement*, vol.54, no.4, augsut 2005.
- R. Olshansky, R. D. Maurer, "Tensile strength and fatigue of optical fibers", *Journal of Applied Physics*, pp. 4497-4499, Vol. 47, N° 10, October 1976.
- A. Othonos, "Fiber Bragg gratings," *Rev. Sci. Instrum*, N°.68, 1997, pp. 43094341, 1997.
- J. A. Gallego-Juarez, "Piezoelectric ceramics and ultrasonic transducers" *J. Phys. E: Sci. Instrum.* 22, pp. 804-816, (1989).
- S. J. Pember, C. M. France, B. E. Jones, "A multiplexed network of optically powered, addressed and interrogated hybrid resonant sensors", *Sensors and Actuators A*, 46-47, pp. 474-477, 1995.
- D. Persegol, J.L. Lovato and V. Minier, "Thermal diagnosis of medium voltage switchboards: a cost-effective multi-pointPOF sensor", 8<sup>th</sup> POF'99, p. 256-259, Chiba, Japan (1999).
- R. M. Ribeiro, L.A. Marques-Filho and M.M. Werneck, "Fluorescent plastic optical fibers for temperature monitoring", 12<sup>th</sup> POF'03, p. 282-285, Seattle, USA (2003).
- B. Ribeiro and M. M. Werneck, "Tensile Response of re-coated Optical Fibers using a recoating machine" *XXXIII Brazilian Meeting on Condensed Matter Physics*, May 2010.

- T. Sawa, K. Kurosawa, T. Kaminishi and T. Yokota, "Development of optical instrument transformers", *IEEE Transactions on Power Delivery* Vol. 5, No. 2, pp. 884-891, April 1990.
- A. Tardy, A. Derossis and J. P. Dupraz, "A current sensor remotely powered and monitored through an optical fiber link", *Optical Fiber Technology*, vol. 1, pp. 181-185, 1995.
- M. M. Werneck, C. C. Carvalho, Ricardo M. Ribeiro and Fernando L. Maciel, "High-voltage current sensing based hybrid technology". Proceedings of the 12th International POF Conference 2003, pp 50-53, University of Washington, Seattle, EUA, September 14-17, 2003.
- M. M. Werneck, A. C. S. Abrantes, "Fiber-optic-based current and voltage measuring system for high-voltage distribution lines", *IEEE Transactions on Power Delivery* 19 (3): 947-951 Jul 2004.
- J. G. Werthen, A. G. Andersson, S. T. Weiss and H. O. Björklund, "Current measurements using optical power", *IEEE Transmission and Distribution Conference*, 1996, pp. 213-218.
- J. G. Werthen, M. Cohen, "Photonic power: delivering power over fiber for optical networks", *International Conference on Photonics in Switching*, Oct. 2006.
- Y. Yao and B. Yi, "FBG Based Voltage Measurement using PZT Modulation," *International Conference Wireless Communications, Networking and Mobile Computing*, pp. 1-4, September 2006.

IntechOpen



### **Modern Telemetry**

Edited by Dr. Ondrej Krejcar

ISBN 978-953-307-415-3

Hard cover, 470 pages

**Publisher** InTech

**Published online** 05, October, 2011

**Published in print edition** October, 2011

Telemetry is based on knowledge of various disciplines like Electronics, Measurement, Control and Communication along with their combination. This fact leads to a need of studying and understanding of these principles before the usage of Telemetry on selected problem solving. Spending time is however many times returned in form of obtained data or knowledge which telemetry system can provide. Usage of telemetry can be found in many areas from military through biomedical to real medical applications. Modern way to create a wireless sensors remotely connected to central system with artificial intelligence provide many new, sometimes unusual ways to get a knowledge about remote objects behaviour. This book is intended to present some new up to date accesses to telemetry problems solving by use of new sensors conceptions, new wireless transfer or communication techniques, data collection or processing techniques as well as several real use case scenarios describing model examples. Most of book chapters deals with many real cases of telemetry issues which can be used as a cookbooks for your own telemetry related problems.

### **How to reference**

In order to correctly reference this scholarly work, feel free to copy and paste the following:

Marcelo M. Werneck and Regina Célia S. B. Allil (2011). Optical Fiber Sensors, Modern Telemetry, Dr. Ondrej Krejcar (Ed.), ISBN: 978-953-307-415-3, InTech, Available from: <http://www.intechopen.com/books/modern-telemetry/optical-fiber-sensors>

**INTECH**  
open science | open minds

### **InTech Europe**

University Campus STeP Ri  
Slavka Krautzeka 83/A  
51000 Rijeka, Croatia  
Phone: +385 (51) 770 447  
Fax: +385 (51) 686 166  
[www.intechopen.com](http://www.intechopen.com)

### **InTech China**

Unit 405, Office Block, Hotel Equatorial Shanghai  
No.65, Yan An Road (West), Shanghai, 200040, China  
中国上海市延安西路65号上海国际贵都大饭店办公楼405单元  
Phone: +86-21-62489820  
Fax: +86-21-62489821



© 2011 The Author(s). Licensee IntechOpen. This is an open access article distributed under the terms of the [Creative Commons Attribution 3.0 License](https://creativecommons.org/licenses/by/3.0/), which permits unrestricted use, distribution, and reproduction in any medium, provided the original work is properly cited.

IntechOpen

IntechOpen